Coherent interaction between light and mechanics

CONTENTS

$\frac{1}{4.1}$	Strong	g coupling			
4.2	Optical cooling of mechanical motion			96	
	$4.\overline{2}.1$	Effective temperature of the optical bath		97	
		4.2.1.1	Coupling to both optical and		
			mechanical baths	103	
	4.2.2	Resolved sideband regime		105	
		4.2.2.1	Weak coupling regime	107	
		4.2.2.2	Strong coupling regime	109	
		4.2.2.3	Mechanical occupancy achieved via		
			resolved sideband cooling in the		
			rotating wave approximation	111	
		4.2.2.4	Approaching the ground state	111	
		4.2.2.5	Thermodynamical understanding of		
			optical cooling	112	
4.3	Optomechanically induced transparency			114	
	4.3.1	Hamiltonian 1			
	4.3.2	Optomechanically induced absorption		116	
		4.3.2.1	Output field	118	
	4.3.3	Optomechanically induced transparency using a			
		double-side	ed optical cavity	119	
		4.3.3.1	Noise performance	121	
		4.3.3.2	Experimental implementation	122	
4.4	Optomechanical entanglement			122	
	4.4.1	Hamiltonian and equations of motion			
	4.4.2	Bogoliubov modes 1			
	4.4.3	Optical and	d mechanical modes in the stable regime	126	

94 ■ Quantum optomechanics

	4.4.4	Einstein-Podolsky-Rosen entanglement	127	
	4.4.5	Covariance matrix		
	4.4.6	Identifying and quantifying entanglement	128	
	4.4.7	Entanglement between intracavity field and		
		mechanical oscillator	129	
	4.4.8	Entanglement of the mechanical oscillator with the		
		external field	133	
		4.4.8.1 Wiener filtering	134	
4.5	Mechanical squeezing of light			
	4.5.1	Basic concept	141	
	4.5.2	Understanding ponderomotive squeezing via the		
		polaron transformation		
		4.5.2.1 Polaron transformation	142	
		4.5.2.2 Squeezing action in the polaron picture	143	
		4.5.2.3 Interaction with the coherent drive and		
		the optical and mechanical baths	144	
	4.5.3	Squeezing spectra	145	

In the previous chapter we examined the linearised radiation pressure interaction between the optical field and mechanical oscillator in a cavity optomechanical system in the case that the optical cavity is coherently driven on resonance. This chapter introduces radiation pressure-based coherent coupling between light and a mechanical oscillator that occurs when an optical detuning is introduced. We discuss effects such as resolved sideband cooling, optomechanically induced transparency, and the generation of optomechanical entanglement and squeezed states of light that manifest from this coherent interaction. Along the way we introduce the concepts of Wiener filtering to optimally estimate the mechanical position and momentum from the output optical field, methods to verify and quantify two-mode Gaussian entanglement, and the polaron transformation important for later chapters involving single photon optomechanics.

4.1 STRONG COUPLING

As a prelude to optomechanical cooling, it is illustrative to examine the dissipation-free dynamics generated by the linearised optomechanical Hamiltonian of Eq. (2.41) in the special case where the optical detuning equals the mechanical resonance frequency ($\Delta = \Omega$). The "X-X" form of the coupling term in this Hamiltonian brings to mind the simple problem of a pair of linearly coupled oscillators. Indeed, this is the essential physics described by the Hamiltonian. The choice of $\Delta = \Omega$, such that the driving laser field is detuned to the red side of the optical resonance by the mechanical resonance frequency,

makes the effective resonance frequencies of the two oscillators degenerate,¹ such that they couple most effectively. Expressed in terms of annihilation operators, the optomechanical Hamiltonian is then

$$\hat{H} = \hbar \Omega a^{\dagger} a + \hbar \Omega b^{\dagger} b + \hbar g \left(a^{\dagger} + a \right) \left(b^{\dagger} + b \right), \tag{4.1}$$

where as usual q is the coherent amplitude boosted optomechanical coupling rate. This fully symmetric Hamiltonian may be straightforwardly diagonalised by transforming to the normal modes

$$c = \frac{1}{\sqrt{2}} \left(a + b \right) \tag{4.2}$$

$$d = \frac{1}{\sqrt{2}} \left(a - b \right), \tag{4.3}$$

where it is easy to show c and d preserve the Boson commutation properties of a and b (Eq. (1.2)). Substituting in for a and b in the Hamiltonian and expanding, after some work we find

$$\hat{H} = \hbar (\Omega + g) c^{\dagger} c + \hbar (\Omega - g) d^{\dagger} d. \tag{4.4}$$

Exercise 4.1 Show this result.

Several important facts can be gleaned from this expression. First, in this normal mode basis the Hamiltonian is indeed diagonalised, with the interaction between the modes removed and the dynamics of the system consequently substantially simplified. Second, c and d are a pair of independent quantum harmonic oscillators. Finally, the original coupling between modes a and bis replaced with opposing frequencies shifts on c and d, resulting in a frequency splitting of 2q between these modes (see experimental demonstration in Fig. 4.6).

In the time domain, c and d then exhibit simple harmonic oscillation with the well-known dynamics²

$$c(t) = c(0)e^{-i(\Omega+g)t}$$

$$d(t) = d(0)e^{-i(\Omega-g)t}.$$

$$(4.5a)$$

$$(4.5b)$$

$$d(t) = d(0)e^{-i(\Omega - g)t}. \tag{4.5b}$$

Using $b = (c - d)/\sqrt{2}$ the dynamics of the mechanical oscillator can then be shown to be

$$b(t) = [b(0)\cos gt - ia(0)\sin gt]e^{-i\Omega t}$$
(4.6)

$$= b^{(0)}(t)\cos gt - ia^{(0)}(t)\sin gt, \tag{4.7}$$

where $a^{(0)}(t)$ and $b^{(0)}(t)$ are the annihilation operators that would describe the time evolution of the intracavity optical field and mechanical oscillator if

¹Remember that, in Eq. (2.41), the optical field is in a rotating frame at the drive laser

²This can be shown, for example, using Eq. (1.20).

there was no optomechanical coupling (g=0). A similar calculation for the optical field gives

$$a(t) = a^{(0)}(t)\cos gt - ib^{(0)}(t)\sin gt. \tag{4.8}$$

We see that, setting an optical detuning $\Delta = \Omega$, the optomechanical interaction allows the quantum state of the light and mechanical oscillator to be coherently and unitarily exchanged.

Of course, in the realistic scenario where dissipation is present, the exchange becomes imperfect. It is natural to then define two physical regimes, the strong coupling and quantum-coherent coupling regimes.³ In the strong coupling regime $q > \{\kappa, \Gamma\}$, so that a full exchange between light and oscillator occurs within the mechanical and optical decay times and the non-degeneracy between normal modes is spectrally resolvable. In the quantum-coherent coupling regime $g > \{(2\bar{n}_L + 1)\kappa, (2\bar{n} + 1)\Gamma\}$ where \bar{n} and \bar{n}_L are the mechanical and optical bath mean occupancies, so that a full exchange between light and oscillator occurs within the quantum decoherence time of both the light and mechanical oscillator (see Section 2.5). The strong coupling and quantumcoherent coupling regimes were first experimentally realised in [130] and [295], respectively.

Notably, if $qt = \pi/2$ the optical and mechanical states are, in the dissipationless scenario of Eqs. (4.7) and (4.8), exactly exchanged. A continuous version of this state-swap is discussed in Section 8.3 as a method to realise quantum conversion between optical and microwave degrees of freedom. Even if the light is only in a relatively uninteresting coherent state, ⁴ a state-swap allows ground state cooling of the mechanical oscillator, with the typically high thermal occupancy mechanical state swapped out onto the optical field and the near zero thermal occupancy optical state swapped onto the mechanical oscillator. In the following section, we introduce a continuous version of this approach to mechanical cooling, including dissipative processes that act to limit the final mechanical occupancy.

4.2 OPTICAL COOLING OF MECHANICAL MOTION

In the previous chapter we introduced on-resonance ($\Delta = 0$) optical probing of mechanical motion, and showed that radiation pressure shot noise heats the mechanical oscillator. This back-action heating is a consequence of the fact that information about the mechanical motion is imprinted on the phase of the optical field, and is necessary to ensure that the Heisenberg uncertainty principle is not violated. However, as the simple example in the previous section

³Note that these regimes are different from the radiation pressure shot noise dominated regime introduced in Section 3.2, which requires that the optomechanical cooperativity $C \equiv 4g^2/\kappa\Gamma > \bar{n} + 1/2$. This radiation pressure shot noise dominated regime lies between the strong coupling and quantum-coherent coupling regimes.

⁴So that, in the displaced frame used in the linearised picture, it is in a vacuum state.

demonstrated, the presence of back-action heating does not necessarily preclude an overall optical cooling effect on the mechanical oscillator. Indeed as we saw briefly in Section 3.2.2, the mapping of the mechanical motion onto the intracavity field suggests a possible a cooling mechanism when $\Delta \neq 0$ based on dynamical back-action. The essential idea is that, when the optical cavity is detuned, the mechanical position is imprinted – at least in part – on the amplitude of the optical field which then back-acts through radiation pressure upon the mechanical oscillator. Since the optical cavity also induces a delay in the optical response, this dynamical back-action is retarded, with a component of the optical force being proportional to the velocity of the mechanical oscillator. Depending on the sign of this component, it either damps/cools or amplifies/heats the mechanical motion [37, 160].

An alternative and particularly powerful approach to understanding optomechanical cooling – and indeed coherent interactions between light and mechanical systems in general – is via an energy level diagram, as shown in Fig. 4.1. Here we observe that downwards going phonon number transitions are resonantly enhanced when the optical driving tone is red detuned, while upwards going transitions are enhanced by blue detuning. We will see in what follows that these two operations can be thought of, respectively, as beam splitting and parametric operations between the light and mechanical oscillator, with the former allowing cooling while the latter can be used to generate optomechanical entanglement.

4.2.1 Effective temperature of the optical bath

The optical field can be thought of as a thermal bath for the mechanical oscillator in a cavity optomechanical system, with radiation pressure shot noise introducing a random driving force (see, e.g., Section 3.3.1). We found in Section 1.2 that the temperature of a high-quality quantum oscillator that is linearly forced by a bath is governed by the ratio of bath power spectral densities at $\pm\Omega$. This relationship provides an elegant approach to determining the effect of the optical field on the temperature of the oscillator, as first observed in [191]. We follow the approach in that paper here.

To understand the effect of the optical field on the temperature of the mechanical oscillator, it is useful to consider first the case where the mechanical oscillator has zero intrinsic dissipation $(\Gamma \to 0)$, or at least where the heating from the optical field dominates the heating from the mechanical bath.⁵ In this case, the optical force makes the only significant contribution towards the force power spectral density experienced by the mechanical oscillator. In Section 3.3.1 we found the optical force \hat{F}_L in a cavity optomechanical system in the linearised regime by taking the derivative of the optomechanical Hamiltonian with respect to \hat{q} . Here, we similarly use the nonlinearised Hamiltonian

⁵That is, in the regime where radiation pressure shot noise dominates mechanical thermal noise.

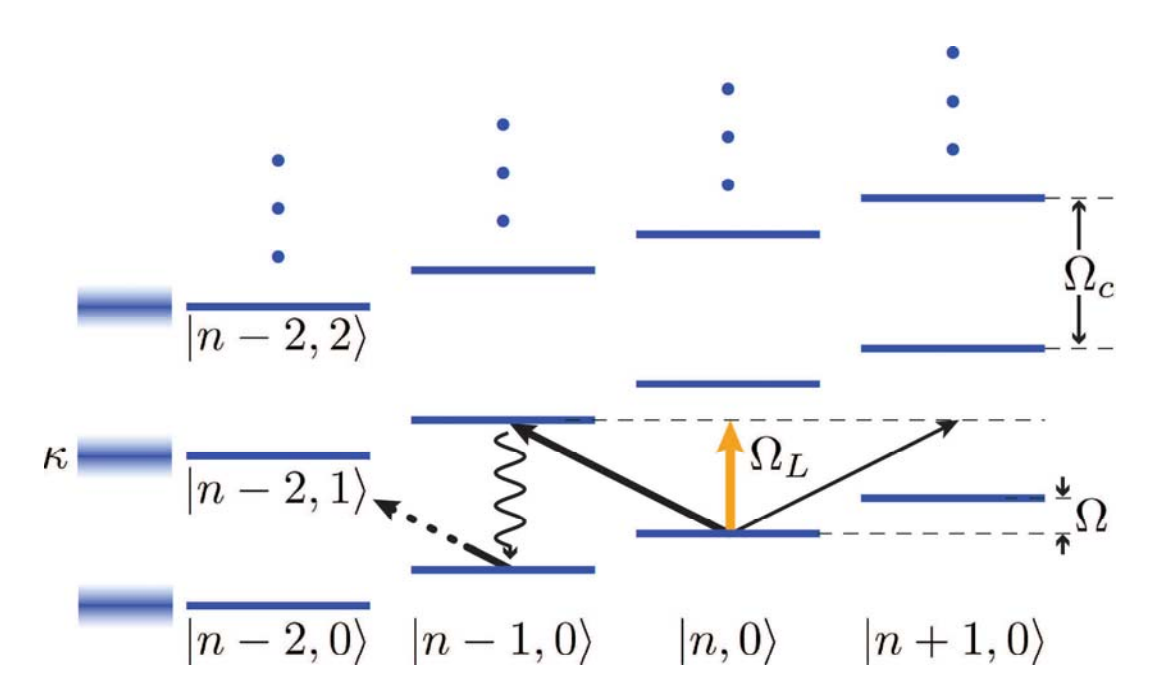


FIGURE 4.1 Energy level diagram for optical cooling of mechanical motion. $|n,m\rangle$: n-phonon, m-photon state. Ω_c : cavity resonance frequency, Ω_L : laser resonance frequency. Laser driving at frequency $\Omega_L < \Omega_c$ is closer to resonance for mechanical cooling transitions $|n,m\rangle \to |n-1,m+1\rangle$ than heating transitions $|n,m\rangle \to |n+1,m-1\rangle$, resulting in preferential cooling. In the resolved sideband limit where $\kappa \ll \Omega$, optimal cooling is achieved when $\Delta = \Omega_c - \Omega_L = \Omega$.

of Eq. (2.15) to obtain the force

$$\hat{F}_L(t) = \frac{\partial \hat{H}}{\partial \hat{q}} = \hbar G a^{\dagger} a. \tag{4.9}$$

The power spectral density of this force can be found from its autocorrelation function (see Eq. (1.43)), which is given by

$$\left\langle \hat{F}_L(t+\tau)\hat{F}_L(t) \right\rangle_{t=0} = \hbar^2 G^2 \left\langle a^{\dagger}(t+\tau)a(t+\tau)a^{\dagger}(t)a(t) \right\rangle_{t=0}$$

$$\approx \frac{\hbar^2 g^2}{x_{zp}^2} \left[\alpha^2 + 2\bar{n}_L + 2 \left\langle \hat{X}(t+\tau)\hat{X}(t) \right\rangle_{t=0} \right].$$
(4.10)

Here, we have made the usual substitution $a \to \alpha + a$ to displace away the coherent amplitude of the intracavity field, linearised the resulting expression by neglecting the term that does not contain the coherent amplitude α , substituted $\alpha G = \alpha g_0/x_{zp} = g/x_{zp}$ (see Section 2.3), and used the relation

 $\langle a^{\dagger}(t)a(t)\rangle = \bar{n}_L$ with \bar{n}_L being the thermal occupancy of the displaced⁶ incident optical field. As usual \hat{X} is the amplitude quadrature of the intracavity field.

Exercise 4.2 Derive this result for yourself.

As we have discussed previously, for an optical field in thermal equilibrium with its environment, \bar{n}_L is given by Eq. (1.7) and is essentially zero. Here we retain the optical occupancy explicitly, motivated both by the aim of clarifying the effect of a nonzero optical bath temperature and by the fact that, in realistic experiments, technical noise often raises the optical occupancy above its equilibrium value.

The optical force power spectral density can then be directly calculated using Eq. (1.43), with the result

$$S_{F_L F_L}(\omega) = \frac{\hbar^2 g^2}{x_{zp}^2} \left[\left(\alpha^2 + 2\bar{n}_L \right) \delta(\omega) + 2S_{XX}(\omega) \right]. \tag{4.11}$$

As might be expected, we see that this consists of a coherent mean force at $\omega =$ 0 and broadband incoherent noise driving due to the amplitude quadrature power spectral density of the intracavity field. It is through this broadband incoherent forcing that the optical field acts like a thermal bath.

Using Eq. (1.43) the power spectral density of the intracavity field can be expressed in terms of frequency domain annihilation and creation operators as

$$S_{XX}(\omega) = \int_{-\infty}^{\infty} d\omega' \left\langle \hat{X}^{\dagger}(-\omega)\hat{X}(\omega') \right\rangle$$

$$= \frac{1}{2} \int_{-\infty}^{\infty} d\omega' \left\langle \left(a(\omega) + a^{\dagger}(-\omega) \right) \left(a^{\dagger}(-\omega') + a(\omega') \right) \right\rangle.$$
 (4.12)

To find an analytical expression for this power spectral density, we must determine $a(\omega)$ and $a^{\dagger}(\omega)$. To do this we use the Hamiltonian of Eq. (2.18) in the rotating wave quantum Langevin equation (Eq. (1.112)). We simplify the problem by making one substantial approximation – that the intracavity optical field is not affected by the motion of the mechanical oscillator (i.e., we set $q_0 = 0$). This may seem like an unreasonable approximation on the face of it. However, it is appropriate as long as the optical cavity decay rate κ is sufficiently large to remove the fluctuations introduced to the optical field by the interaction with the mechanical oscillator. We will consider the case where this is not true in Section 4.2.2, where we find that the approximation is reasonable as long as κ is large enough that the optomechanical system is not operating within the strong coupling regime (i.e., $\kappa \gg g$).

Returning to the problem at hand, setting $g_0 = 0$ and taking the Fourier

⁶That is, the thermal occupancy if the coherent driving tone is displaced away.

transform of the equation of motion for the intracavity optical field, we find

$$a(\omega) = \frac{\sqrt{\kappa}}{\kappa/2 + i(\Delta - \omega)} a_{\rm in}(\omega) = \chi_{\rm opt}(\omega) a_{\rm in}(\omega), \tag{4.14}$$

where, in the same spirit as the mechanical susceptibility $\chi(\omega)$, we have quantified the frequency response of the optical cavity via the *optical susceptibility*

$$\chi_{\text{opt}}(\omega) = \frac{\sqrt{\kappa}}{\kappa/2 + i(\Delta - \omega)}.$$
(4.15)

Substituting Eq. (4.14) into Eq. (4.13) and using the bath correlation relations properties in Eqs. (1.115a) and (1.115c), which are valid for our model of the optical bath since we have taken a rotating wave approximation, we then find that

$$S_{XX}(\omega) = \frac{1}{2} \left[\bar{n}_L |\chi_{\text{opt}}(-\omega)|^2 + (\bar{n}_L + 1) |\chi_{\text{opt}}(\omega)|^2 \right].$$
 (4.16)

Exercise 4.3 Show this result.

It is notable that this optical amplitude quadrature spectral density is asymmetric in frequency. As discussed in Section 1.2.3, this is a key signature that the, in this case optical, bath is acting to heat or cool the mechanical oscillator. Neglecting the coherent driving term at $\omega = 0$, which acts only to statically displace the mechanical oscillator, we can now establish an analytical expression for the optical force power spectral density of Eq. (4.11):

$$S_{F_L F_L}(\omega) = \frac{\hbar^2 g^2}{x_{zp}^2} \left[\bar{n}_L |\chi_{\text{opt}}(-\omega)|^2 + (\bar{n}_L + 1) |\chi_{\text{opt}}(\omega)|^2 \right]. \tag{4.17}$$

If the optical force is the only appreciable source of heating of the mechanical oscillator and the mechanical oscillator has sufficiently high quality that $S_{F_LF_L}(\omega)$ is flat across the mechanical resonance, the equilibrium phonon occupancy \bar{n}_b and the optically induced mechanical decay rate $\Gamma_{\rm opt}$ can be determined by substitution of Eq. (4.17), respectively, into Eqs. (1.54b) and (1.62). Note that, since Eq. (1.54b) is a ratio of the power spectral densities at $\pm \Omega$, the prefactor in Eq. (4.17) plays no role in determining the equilibrium phonon occupancy, with the occupancy determined solely by the characteristics of the optical field. The results of these substitutions are

$$\Gamma_{\text{opt}} = g^{2} \left[|\chi_{\text{opt}}(\Omega)|^{2} - |\chi_{\text{opt}}(-\Omega)|^{2} \right]$$

$$\bar{n}_{b,\text{opt}} = \frac{g^{2}}{\Gamma_{\text{opt}}} \left[\bar{n}_{L} |\chi_{\text{opt}}(\Omega)|^{2} + (\bar{n}_{L} + 1) |\chi_{\text{opt}}(-\Omega)|^{2} \right]$$

$$= \frac{\bar{n}_{L} |\chi_{\text{opt}}(\Omega)|^{2} + (\bar{n}_{L} + 1) |\chi_{\text{opt}}(-\Omega)|^{2}}{|\chi_{\text{opt}}(\Omega)|^{2} - |\chi_{\text{opt}}(-\Omega)|^{2}}.$$
(4.18b)

To understand these relations, it is worthwhile to consider three specific scenarios:

- If the optical driving field is on resonance $(\Delta = 0)$, $|\chi_{\rm opt}(\omega)| =$ $|\chi_{\rm opt}(-\omega)|$, so that the optically induced mechanical decay rate $\Gamma_{\rm opt}=0$ and $\bar{n}_{b,\text{opt}} = \infty$. Consistent with our observations from Section 3.2, in this regime the optical field causes heating and does not affect the mechanical damping rate. Since, in our current model the mechanical oscillator is not directly coupled to any other bath, there is no mechanical decay, so that the steady-state temperature is infinite.
- If the optical field is blue detuned $(\Delta < 0)$, $|\chi_{\rm opt}(-\omega)| > |\chi_{\rm opt}(\omega)|$ so that $\{\Gamma_{\text{opt}}, \bar{n}_{b,\text{opt}}\} < 0$. In this case, each photon impinging on the optical cavity carries more energy than an intracavity photon. To enter the cavity, a scattering process must occur whereby the mechanical oscillator takes up some of the photons' energy (see Fig. 4.1). As a result, the optical field coherently adds energy to the mechanical oscillator, providing gain (or negative damping) to its motion. Since the mechanical oscillator has no other pathway to lose energy, its energy exponentially grows. The fact that $\bar{n}_{b,\text{opt}}$ is negative in this situation can be understood because the power spectral density of the optical bath that it is coupled to increases with frequency – the opposite behaviour to that of a system in thermal equilibrium. This results in an effective negative temperature within the Boltzmann factor (see Eq. (1.54b)).
- If the optical field is red detuned $(\Delta > 0)$, $|\chi_{\rm opt}(-\omega)| < |\chi_{\rm opt}(\omega)|$ so that $\{\Gamma_{\text{opt}}, \bar{n}_{b,\text{opt}}\} > 0$. This is the reverse situation to that discussed above, with each incident optical photon carrying less energy than an intracavity photon. As a result, scattering processes cause a net optical damping of the mechanical oscillator, which then reaches a finite positive equilibrium phonon occupancy.

We examine the last of these three scenarios in detail in what follows.

Figure 4.2 shows the optically induced mechanical damping rate $\Gamma_{\rm opt}$ as a function of detuning for a range of resolved sideband parameters Ω/κ . It can be seen that, indeed, additional damping is introduced for $\Delta > 0$, and negative damping (or amplification) is introduced for $\Delta < 0$. The maximum damping/amplification occurs near detunings equal to $\Delta = \pm \Omega$, with the range of frequencies that achieve effective damping/amplification narrowing to small regions around these detunings as the resolved sideband factor Ω/κ increases. This can be readily understood, because when $\Delta = \pm \Omega$ the scattering process that transfers energy between the optical field and the mechanical oscillator is resonant (see Fig. 4.1). Taking this special resonant case while

⁷It should be noted that, while the vertical axis of Fig. 4.2 is normalised to the optomechanical coupling rate q, in practise for a fixed incident optical power q is a function of the detuning Δ . As the detuning increases away from resonance for fixed incident power, the intracavity phonon number, and therefore q, is reduced. Taking this into account, one finds that, outside of the well-resolved sideband regime where $\Omega/\kappa \gg 1$, the detuning at which maximum optical damping/amplification occurs is shifted towards resonance (i.e., $|\Delta| < \Omega$).

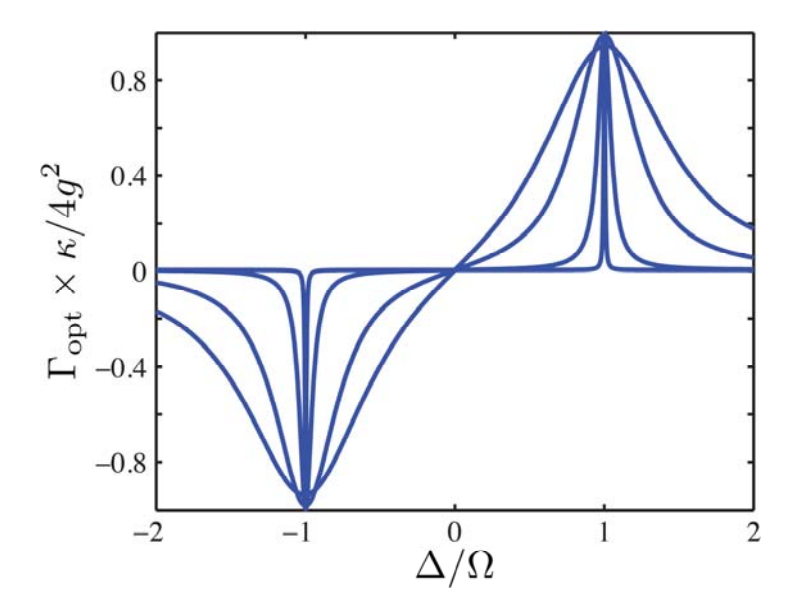


FIGURE 4.2 Optically induced mechanical damping rate $\Gamma_{\rm opt}$ as a function of cavity detuning Δ for resolved sideband ratios $\Omega/\kappa = \{1, 2, 10, 100\}$ in order of least to most sharply peaked curve.

driving on the red (cooling) side of the optical resonance ($\Delta = \Omega$), we find

$$\Gamma_{\text{opt}}^{\Delta=\Omega} = \frac{4g^2}{\kappa} \left[1 + \left(\frac{\kappa}{4\Omega} \right)^2 \right]^{-1}$$
(4.19a)

$$\bar{n}_{b,\text{opt}}^{\Delta=\Omega} = \bar{n}_L + \left(\frac{\kappa}{4\Omega}\right)^2 (2\bar{n}_L + 1),$$

$$(4.19b)$$

This is exactly the scenario we considered in Section 4.1, where we showed that, with this detuning, the state of the optical field and mechanical oscillator swap at the rate 2g. It is perhaps unsurprising, therefore, to find that this results in cooling of the mechanical oscillator. We observe from Eq. (4.19b) that, in the resolved sideband regime ($\kappa \ll \Omega$), the mechanical oscillator equilibrates to the occupancy of the optical field ($\bar{n}_{b,\text{opt}}^{\Delta=\Omega}=\bar{n}_L$), with additional deleterious heating introduced as the resolved sideband factor decreases. If light is shot-noise limited ($\bar{n}_L=0$), this additional heating introduces the fundamental limit [191, 314]

$$\bar{n}_{b,\text{opt}}^{\Delta=\Omega} = \left(\frac{\kappa}{4\Omega}\right)^2 \tag{4.20}$$

on the mechanical occupancy. Thus we see that, somewhat surprisingly, even when using an ideal minimum uncertainty coherent state to drive the optomechanical system, the presence of an optical cavity causes the optical field to act like a nonzero temperature bath for the mechanical oscillator.

4.2.1.1 Coupling to both optical and mechanical baths

In most scenarios, with the notable exception of laser trapped atoms, it is not realistic to neglect the coupling of the mechanical oscillator to its mechanical bath. In general, if the oscillator is coupled to two independent baths (labelled A and B here), the total force power spectral density that it experiences is simply

$$S_{FF}(\omega) = S_{FF}^{A}(\omega) + S_{FF}^{B}(\omega). \tag{4.21}$$

From Eqs. (1.54b) and (1.62) the equilibrium phonon occupancy of the oscillator is then just the weighted mean

$$\bar{n}_b = \left(\frac{x_{zp}}{\hbar}\right)^2 \left[\frac{S_{FF}^A(-\Omega) + S_{FF}^B(-\Omega)}{\Gamma_A + \Gamma_B}\right] \tag{4.22}$$

$$= \frac{\Gamma_A \bar{n}_b^A + \Gamma_B \bar{n}_b^B}{\Gamma_A + \Gamma_B}, \tag{4.23}$$

where \bar{n}_b^A and \bar{n}_b^B , and Γ_A and Γ_B , are the phonon occupancies and damping rates, respectively, that would be obtained if the baths were individually coupled to the oscillator, as defined by Eqs. (4.18a) and (4.18b).

Exercise 4.4 Show this result.

Substituting the optical and mechanical parameters from earlier ($\{\bar{n}_A, \bar{n}_B\} \rightarrow \{\bar{n}_{b,\text{opt}}, \bar{n}\}$, $\{\Gamma_A, \Gamma_B\} \rightarrow \{\Gamma_{\text{opt}}, \Gamma\}$) into Eq. (4.23), it is then possible to analytically determine the equilibrium mechanical occupancy in the presence of both optical and mechanical baths, remembering that the result is only valid outside of the optomechanical strong coupling limit (specifically in the regime where $\kappa \ll g$).

Exercise 4.5 Derive the analytic expression for yourself. Show that onresonance optical driving $(\Delta = 0)$ heats the mechanical oscillator without altering its decay rate and results in an equilibrium occupancy of

$$\bar{n}_b = \bar{n} + |C_{\text{eff}}| (2\bar{n}_L + 1),$$
 (4.24)

where $C_{\rm eff}$ is the effective cooperativity defined in Eq. (3.13), consistent with what we found in Section 3.2.

The equilibrium mechanical occupancy is plotted as a function of optical detuning in Fig. 4.3 for a range of optomechanical cooperativities C. As can be seen, when $|\Delta| \gg \Omega$ the mechanical occupancy asymptotes to \bar{n} as expected. Net optical heating occurs for $\Delta < 0$, with the system exhibiting instability over the range of detunings for which $\Gamma_{\rm opt} + \Gamma < 0$. Net cooling beneath the occupancy of the mechanical bath occurs for $\Delta > 0$, and as expected is strongly peaked near $\Delta = \Omega$. In this special resonant cooling regime $(\Delta = \Omega)$, if the optical field is treated as a coherent state $(\bar{n}_L = 0)$, we find that the equilibrium occupancy is

$$\bar{n}_b = \frac{\bar{n} + (\kappa/4\Omega)^2 (\bar{n} + C)}{1 + C + (\kappa/4\Omega)^2}.$$
(4.25)

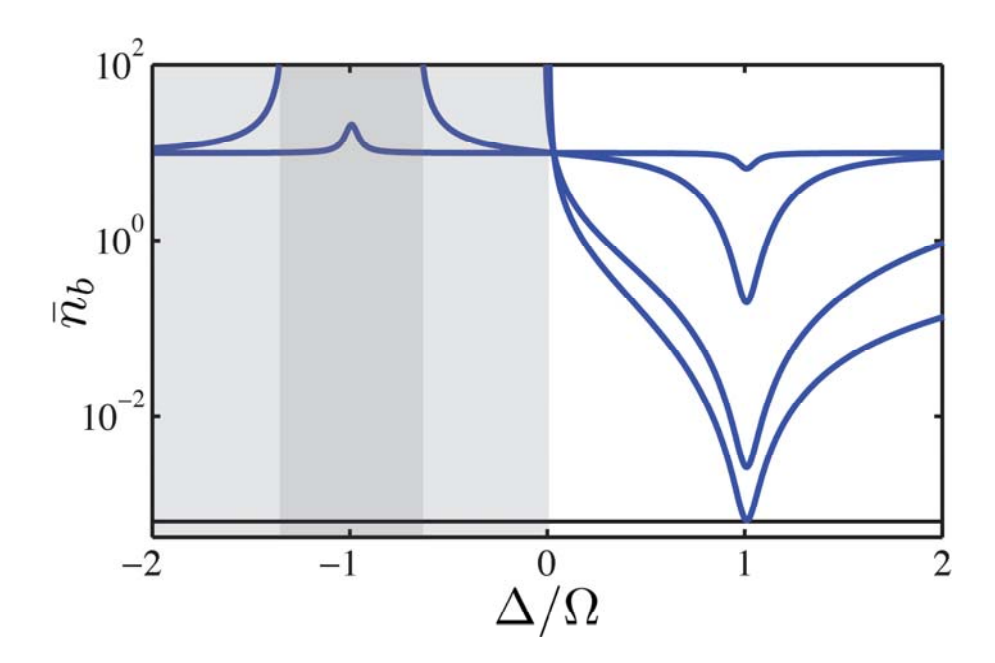


FIGURE 4.3 Optical cooling and amplification of the motion of a mechanical oscillator as a function of detuning Δ for various optomechanical cooperativities. Here the mechanical bath occupancy is $\bar{n}=10$ and the resolved sideband parameter $\Omega/\kappa=10$. The optomechanical cooperativity is $C=\{0.5,50,5\times10^3,5\times10^5\}$ in order of the traces showing the least to most cooling at $\Delta=\Omega$. The thin horizontal line is the fundamental limit due to radiation pressure shot noise heating (Eq. (4.25)). The light shaded region is the region of instability for $C\geq 5000$ and the dark shaded region is the region of instability for C=50.

In the limit where the resolved sideband factor $(\kappa/\Omega)^2 \ll \{\bar{n}/(\bar{n}+C), 1+C\}$, this can be approximated as

$$\bar{n}_b = \frac{\bar{n}}{1+C},\tag{4.26}$$

while in the alternative limit that the optomechanical cooperativity C dominates all other terms $(C \gg \{1 + (\kappa/4\Omega)^2, \bar{n}[(4\Omega/\kappa)^2 + 1]\})$ the mechanical occupancy reaches the fundamental limit set by optical radiation pressure heating given in Eq. (4.20).

In this textbook we will generally define being "close to the ground state" as meaning $\bar{n}_b < 1$. With this definition, we see that, in the first of the above limits, the ground state can be approached for $C > \bar{n} + 1$. Interestingly, in the limit that $\bar{n} \gg 1$, this condition approaches the requirement we found in Section 3.2 for the radiation pressure back-action heating of a mechanical oscillator to equal \bar{n} in the nonresolved sideband limit with on-resonance

optical driving.⁸ The significance of the condition in Section 3.2 is that once $C > \bar{n}$, a measurement on the output field of the optical cavity is able to resolve the zero-point motion of the oscillator in a time shorter than the time one phonon enters from the bath. Here, a similar conclusion may be drawn. When $C > \bar{n} + 1$, the coherent cooling provided by the optomechanical interaction is able to extract the full \bar{n} of occupancy from the mechanical oscillator in a time that is short compared to the time within which one phonon enters from the bath.

4.2.2 Resolved sideband regime

In the previous section, we derived the final temperature of a mechanical oscillator in the presence of both optical and mechanical bath forcing, under the approximation that the optomechanical interaction introduces negligible heating to the intracavity optical field. As we discussed, this approximation is only valid if the optical decay rate κ is sufficiently high that the energy extracted from the mechanical oscillator does not remain in the optical cavity long enough to couple back into the oscillator, i.e., when the optomechanical system is outside of the strong coupling regime (see Section 4.1). In this section we use a quantum Langevin approach to include the effect of this recycling of energy back into the mechanical oscillator, while taking the ideal resolved sideband limit ($\kappa \ll \Omega$) where direct radiation pressure heating of the mechanical oscillator does not significantly raise its temperature (see Eqs. (4.20) and (4.26)). In the resolved sideband regime each intracavity photon on average remains in the cavity for longer than the mechanical period and therefore interacts more or less equally with all quadratures of mechanical motion. The interaction term in the Hamiltonian in Eq. (4.1) may then be simplified by making a rotating wave approximation which neglects the fast oscillating terms (ab and $a^{\dagger}b^{\dagger}$). An alternative way to justify this assumption is by considering the optomechanical energy level diagram in Fig. 4.1. It is clear that the scattering processes described by ab and $a^{\dagger}b^{\dagger}$ are off-resonance and therefore suppressed if $\kappa \ll \Omega$. With this approximation, the Hamiltonian becomes

$$\hat{H} = \hbar \Omega a^{\dagger} a + \hbar \Omega b^{\dagger} b + \hbar g \left(a^{\dagger} b + a b^{\dagger} \right). \tag{4.27}$$

This is a beam splitter Hamiltonian which acts to swap excitations between the mechanical oscillator and the optical field.

Exercise 4.6 Use the quantum Langevin equation given in Eq. (1.112) to find

⁸It should be noted that, while the conditions become identical in this limit, resolved sideband cooling remains much more difficult to achieve in practise. One reason for this is that radiation pressure heating can be achieved with an on-resonance optical drive, while optomechanical cooling requires that the optical field is detuned. As a result, a higher incident optical power is required to achieve the same intracavity optical power (and therefore the same C) in the case of optomechanical cooling.

⁹Therefore, requiring appreciable quantum back-action noise on the mechanical oscillator to sustain the Heisenberg uncertainty principle.

equations of motion for both a and b, valid within the rotating wave approximation. Then solve these equations for b in the frequency domain, ignoring transient boundary terms that arise due to the initial conditions, to obtain the result

$$b(\omega) = \chi_{bb}(\delta) b_{in}(\omega) + \chi_{ba}(\delta) a_{in}(\omega), \tag{4.28}$$

where $\delta = \Omega - \omega$ is the offset frequency from the mechanical resonance frequency, and

$$\chi_{bb}(\delta) = \sqrt{\Gamma} \left[\frac{\kappa/2 + i\delta}{(\Gamma/2 + i\delta)(\kappa/2 + i\delta) + g^2} \right]$$
(4.29a)

$$\chi_{ba}(\delta) = -\sqrt{\kappa} \left[\frac{ig}{(\Gamma/2 + i\delta)(\kappa/2 + i\delta)} \right]$$
(4.29b)

are the mechanical-bath-to-mechanical oscillator and optical-bath-to-mechanical oscillator susceptibilities, respectively.

Equation (4.28) matches our intuition from the unitary approach to strong optomechanical coupling considered in Section 4.1. b is a linear combination of $b_{\rm in}$ and $a_{\rm in}$. The proportion arising from $a_{\rm in}$ is linearly proportional to g, and the proportion arising from $b_{\rm in}$ decreases with g. Hence, in the usual limit where the optical bath occupancy is much lower than the mechanical bath occupancy ($\bar{n}_L \ll \bar{n}$), the optomechanical coupling results in cooling.

For a stationary system, the mean occupancy of the mechanical mode can be calculated from the frequency spectrum of b using Parseval's theorem since

$$\bar{n}_b = \langle b^{\dagger}(t)b(t) \rangle$$
 (4.30)

$$= \lim_{\tau \to \infty} \frac{1}{\tau} \int_{-\tau/2}^{\tau/2} \left\langle b^{\dagger}(t)b(t) \right\rangle dt \tag{4.31}$$

$$= \frac{1}{2\pi} \int_{-\infty}^{\infty} S_{bb}(\omega) d\omega \tag{4.32}$$

$$= \frac{1}{2\pi} \iint_{-\infty}^{\infty} \left\langle b^{\dagger}(\omega)b(\omega') \right\rangle d\omega d\omega', \tag{4.33}$$

where in the first step we have evoked stationarity, in the second used Parseval's theorem, and in the final step used the relation in Eq. (1.43). In the reasonable case that the mechanical and optical baths are uncorrelated, we then find that the mechanical occupancy is

$$\bar{n}_b = \frac{1}{2\pi} \left[\bar{n} \int_{-\infty}^{\infty} |\chi_{bb}(\delta)|^2 d\delta + \bar{n}_L \int_{-\infty}^{\infty} |\chi_{ba}(\delta)|^2 d\delta \right], \tag{4.34}$$

where we have used the frequency domain version of the bath correlation property in Eq. (1.115a), which is valid within the rotating wave approximation.

Exercise 4.7 In the limit of no optomechanical coupling (g = 0) confirm that

 $|\chi_{bb}(\delta)|^2$ is a Lorentzian centred around $\delta = 0$ ($\omega = \Omega$) with a width of Γ . Then show that, as should be expected, in this case the oscillator is equilibrated at the temperature of its environment with $\bar{n}_b = \bar{n}$.

It should be clear from inspection of Eqs. (4.29) that, in general, $|\chi_{bb}(\delta)|^2$ and $|\chi_{ba}(\delta)|^2$ are not Lorentzian. This means that, in general, once an optomechanical interaction is introduced, the mechanical oscillator can no longer be thought of as an isolated mechanical oscillator in thermal equilibrium with its environment. It is still possible, of course, to determine its occupancy via Eq. (4.34). However, the integrals are not straightforward to solve analytically. To simplify matters, henceforth we take the experimentally relevant limit that the optical field is shot-noise limited so that $\bar{n}_L = 0$. In this case Eq. (4.34) reduces to

 $\bar{n}_b = \frac{\bar{n}}{2\pi} \int_{-\infty}^{\infty} |\chi_{bb}(\delta)|^2 d\delta. \tag{4.35}$

To make progress in solving this integral, it is insightful to consider the characteristics of $|\chi_{bb}(\delta)|^2$ as a function of the optomechanical coupling strength. The thick lines in Fig. 4.4 show this. As can be seen, for low optomechanical coupling strengths the form of $|\chi_{bb}(\delta)|^2$ appears to be Lorenzian-like. The function broadens and decreases in amplitude as the optomechanical coupling strength increases, and eventually splits into two peaks separated by 2g. As discussed in Section 4.1, this splitting is a characteristic signature of strong coupling between the intracavity optical field and the mechanical oscillator. These observations motivate us to search for separate approximate forms of $|\chi_{bb}(\delta)|^2$ that are accurate in the strong coupling regime where $g \gg \{\Gamma, \kappa\}$ and in the complimentary weak coupling regime where $\{g, \Gamma\} \ll \kappa$. We would note that, despite its name, the latter regime does not imply that radiation pressure shot noise may be neglected. It can be seen from Eq. (3.19) that, even in the weak coupling regime, radiation pressure shot noise can dominate the heating of the mechanical oscillator.

Exercise 4.8 Convince yourself of this.

4.2.2.1 Weak coupling regime

Considering – in generality – a mechanical oscillator that has a decay rate Γ and is coupled to an optical field with rate g, it can be anticipated that the energy of the oscillator will be predominantly confined to frequencies within $\Gamma + g$ of the mechanical resonance frequency. This presumption leads to the expectation that frequency components outside of the range $|\delta| \lesssim \Gamma + g$ should have little contribution to the integral in Eq. (4.35). In the weak coupling regime where $g \ll \kappa$, and assuming the usual situation where $\Gamma \ll \kappa$, this leads to the conclusion that the only frequencies that contribute significantly to the integral satisfy $|\delta| \ll \kappa$. It is then possible to approximate Eq. (4.29a)

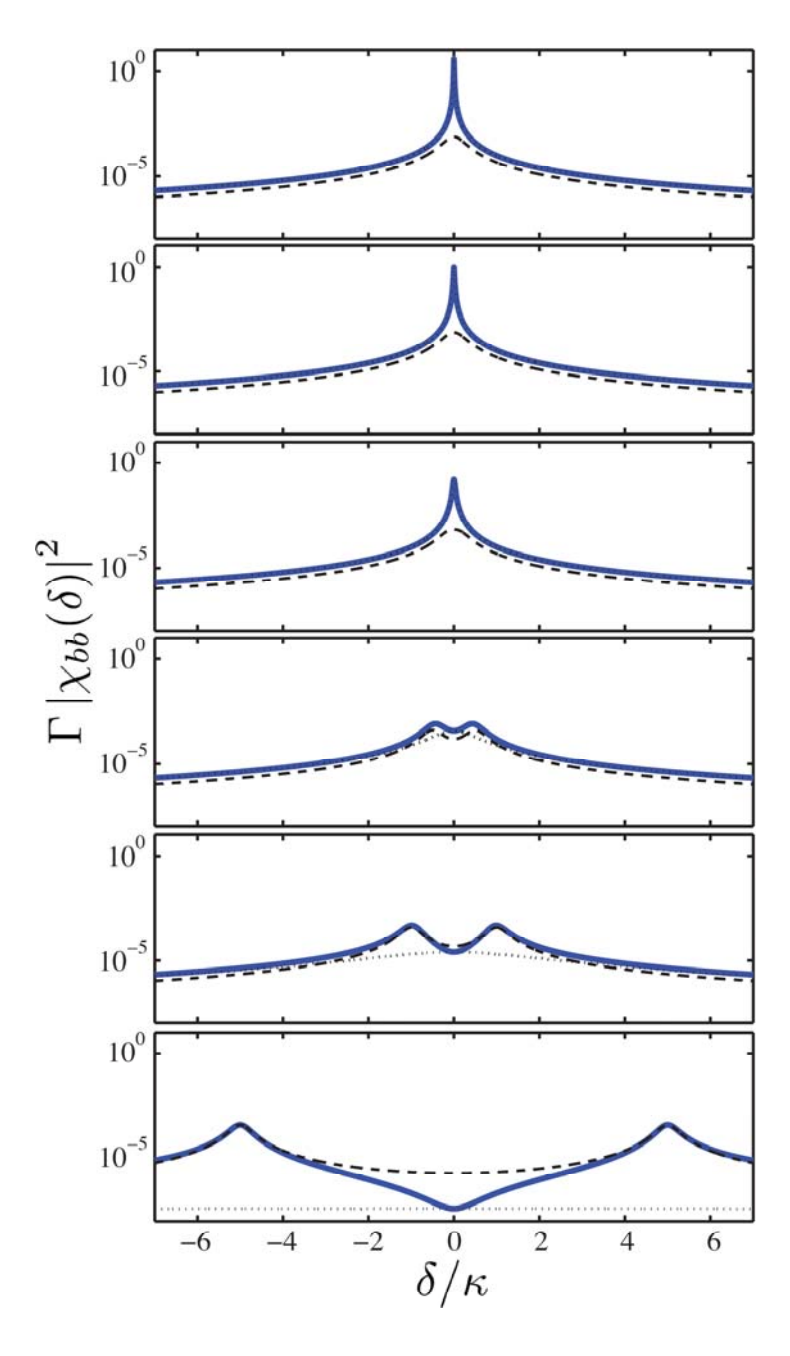


FIGURE 4.4 Modification of the absolute-squared mechanical susceptibility $(|\chi_{bb}(\delta)|^2)$ due to resolved sideband cooling with varying optomechanical coupling strengths. Here $\Gamma/\kappa = 0.01$, and from top to bottom $g/\kappa = \{0, 0.05, 0.1, 0.5, 1, 5\}$, or expressed in terms of the optomechanical cooperativity $C = \{0, 1, 4, 100, 400, 1 \times 10^4\}$. The thick solid lines are predicted from the full model (Eq. (4.29a)), the dotted lines are predicted using the weak-coupling approximation (Eq. (4.37)), and the dashed lines are using the strong coupling approximation (Eq. (4.40)).

as

$$\chi_{bb}(\delta) \approx \frac{\sqrt{\Gamma}}{\Gamma/2 + 2g^2/\kappa + i\delta}$$
(4.36)

$$= \frac{\sqrt{\Gamma}}{\Gamma/2 \times (1+C) + i\delta},\tag{4.37}$$

where C is the usual optomechanical cooperativity of Eq. (3.14). This is, indeed, a Lorenzian with an increased width of

$$\Gamma' = (1+C)\,\Gamma,\tag{4.38}$$

and on-resonance peak height $\chi_{bb}(0)$ reduced compared to the bare mechanical oscillator by a factor of 1 + C.

Exercise 4.9 Show that the optical contribution to Γ' in Eq. (4.38) agrees with Eq. (4.19a) in the very good cavity limit $(\kappa \ll \Omega)$.

Equation (4.37) is illustrated by the dotted lines in Fig. 4.4. In the weak coupling regime the agreement with the full mechanical susceptibility is near perfect, with major discrepancies becoming evident as the strong coupling regime is approached.

Applying this result for $\chi_{bb}(\delta)$ into Eq. (4.35), we find that the mean mechanical occupancy for resolved sideband cooling in the weak coupling limit is

$$\bar{n}_b = \frac{\bar{n}}{1+C}.\tag{4.39}$$

This expression is identical to the result we found earlier (Eq. (4.26)) when neglecting both mechanical heating of the optical field and radiation pressure heating of the mechanical oscillator.

4.2.2.2 Strong coupling regime

As discussed earlier, as the strong coupling regime is approached the mechanical phonon number spectrum characterised by $\chi_{bb}(\delta)$ starts to take on the appearance of a double-peaked Lorenzian (see Figs. 4.4 and 4.6). Each of the peaks represents one of the pair of hybridised optomechanical modes described in Section 4.1. We know from Section 4.1 that the separation of the peaks should equal 2g. In the weak coupling regime the decay of the cavity field is fast compared to the optomechanical coupling rate $(g \ll \kappa)$ such that the heat transfer from the mechanical oscillator into the optical environment is rate-limited by g. Here, on the other hand, since $g \gg \kappa$, the exact opposite is true, with the rate of heat transfer limit by κ . As a result, one should expect the linewidths of the hybrid modes to be determined by κ and Γ rather than g. This leads to the conclusion that frequency components in the mechanical power spectrum that are outside of the ranges $|\delta \pm g| \lesssim \Gamma + \kappa$ should not contribute appreciably to the mechanical occupancy. Using the strong coupling criterion $g \gg \{\kappa, \Gamma\}$, this can be rewritten in the relaxed form $|\delta \pm g| \ll g$.

Returning to the general form of the susceptibility in Eq. (4.29a), and utilising the approximations outlined in the previous paragraph, we find after some work that in the strong coupling regime $|\chi_{bb}(\delta)|^2$ is well approximated by

$$\left|\chi_{bb}(\delta)\right|^2 = \frac{\Gamma/4}{\left(\frac{\Gamma+\kappa}{4}\right)^2 + (\delta+g)^2} + \frac{\Gamma/4}{\left(\frac{\Gamma+\kappa}{4}\right)^2 + (\delta-g)^2}.$$
 (4.40)

Exercise 4.10 Show this for yourself.

This function is represented by the dashed lines in Fig. 4.4, showing good agreement with the full absolute-squared mechanical susceptibility in the strong coupling regime close to the hybrid modes resonance frequencies, and, as should be expected, poor agreement in the weak coupling regime. Unlike the weak measurement regime, here both the height and shape of the Lorenzian peaks are independent of g. Furthermore, since the absolute-squared susceptibility, and therefore the mechanical power spectrum, is not a single Lorenzian, the mechanical oscillator cannot be thought of simply as a single oscillator coupled to a bath in thermal equilibrium. Each hybrid optomechanical mode can, however, be thought of in this way.

As can be seen from Eq. (4.40), the width of each Lorenzian is

$$\Gamma' = \frac{\Gamma + \kappa}{2}.\tag{4.41}$$

This is exactly the usual result for a pair of strongly coupled oscillators: the decay rate of the hybrid modes is the average of the uncoupled decay rates since the energy of each hybrid mode is shared equally between the two oscillators.

Compared with the peak of the bare amplitude-squared mechanical susceptibility when no optomechanical coupling is present, the peak of each of the two Lorenzians in Eq. (4.40) is reduced by the fraction

$$\frac{\left|\chi_{bb}(\delta \pm g)\right|^2}{\left|\chi_{bb}(0)\right|_{q=0}^2} \approx \left(\frac{\Gamma}{\Gamma + \kappa}\right)^2. \tag{4.42}$$

Evidently, this ratio, and consequently the level of mechanical cooling, critically depends on the ratio of mechanical to optical decay rates.

Similarly to the weak coupling regime, integrating Eq. (4.42) over δ yields the occupancy of the mechanical mode in the strong coupling limit, with the result

$$\bar{n}_b = \bar{n} \left(\frac{\Gamma}{\Gamma + \kappa} \right) \approx \bar{n} \left(\frac{\Gamma}{\kappa} \right),$$
 (4.43)

where the approximate solution is valid in the realistic scenario that the optical cavity decays much faster than the mechanical oscillator ($\kappa \gg \Gamma$). We see that, within the strong coupling regime, the final equilibrium occupancy is simply equal to the mechanical bath occupancy suppressed by the ratio of mechanical to optical decay rates.

4.2.2.3 Mechanical occupancy achieved via resolved sideband cooling in the rotating wave approximation

Figure 4.5 provides an example of the reduction in phonon occupancy achieved by resolved sideband cooling in the rotating wave approximation and compares the full numerical integration of Eq. (4.35) with the weak and strong coupling approximations derived in the previous two subsections. As can be seen, good agreement is achieved in the regimes of validity of each model.

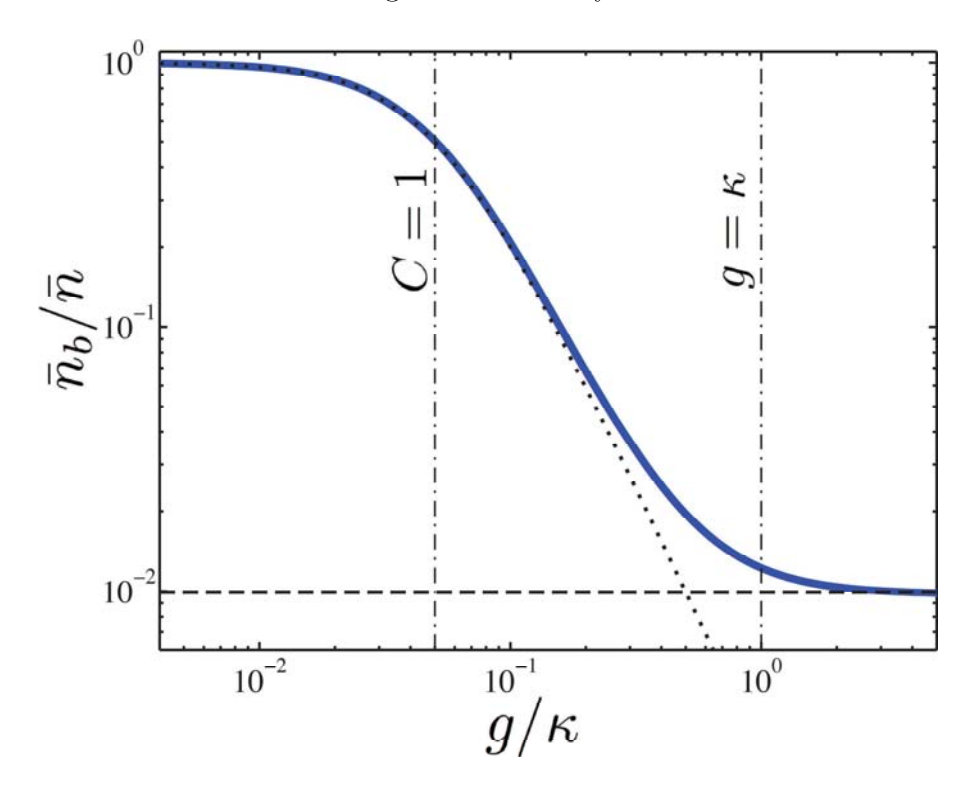


FIGURE 4.5 Final mechanical occupancy achieved with resolved sideband cooling in the rotating wave approximation. Here we set $\Gamma/\kappa = 0.01$. The dotted and dashed lines are the predictions when using the additional weak (Eq. (4.39)) and strong (Eq. (4.43)) coupling approximations, respectively.

Approaching the ground state 4.2.2.4

Optomechanical cooling is a commonly used technique in atom and ion trapping experiments, where operation in the resolved sideband regime routinely enables cooling to the ground state as an initialisation step for experiments in quantum computing and quantum information science [86, 202, 176]. Doppler cooling, on the other hand, is analogous to cavity optomechanical cooling in the nonresolved sideband regime [154].

Optomechanical cooling of a macroscopic mechanical oscillator was first reported in the microwave frequency domain by Braginskii, Manukin, and Tikhonov in 1970, using a radio frequency waveguide resonator with one end consisting of a metal plate suspended on a quartz fibre [38]. The resolved sideband regime was achieved in 1995 using microwave driving and readout of a superconducting high-Q niobium resonant mass gravitational wave antenna [31, 83].

In the optical domain, passive radiation pressure cooling was observed in 2006 [16, 120, 250] in three different microcavity architectures, ¹⁰ and the resolved sideband regime was achieved in 2008 using both microtoroidal and microsphere optomechanical systems [251, 218]. Figure 4.6 shows a resolved sideband cooling experiment performed using a microtoroidal optomechanical system [295], which clearly shows the hybridisation of the optical and mechanical modes that occurs within the strong coupling regime.

From Eqs. (4.20), (4.39), and (4.43), one can see that there are three requirements to approach the ground state via resolved sideband cooling

$$\Gamma \bar{n} \ll \kappa \ll \left\{ \Omega, \frac{g^2}{\Gamma \bar{n}} \right\}.$$
(4.44)

The first requirement arises because the optical cavity decay rate presents a bottleneck on how fast heat can leave the system, the second comes from heating due to the off-resonant fast rotating terms in the Hamiltonian, and the third is a condition on the required strength of optomechanical coupling. Resolved sideband cooling experiments that approached the ground state $(\bar{n}_b < 1)$ were first achieved in 2011, both using a photonic-phononic crystal architecture [66] and using a superconducting lumped element electromechanical system [280].

4.2.2.5 Thermodynamical understanding of optical cooling

In Section 4.2.1.1 we found that the steady-state phonon occupancy of an oscillator coupled to two baths equilibrates to a mean of the occupancies of the baths, weighted by the respective coupling rates to each bath (see Eq. (4.23)). This provides an alternative way to think about – and to derive – the optomechanical cooling results from Sections 4.2.2.1 and 4.2.2.2, requiring only the appropriate choice of bath occupancies and system-bath coupling rates. The mechanical oscillator is, of course, coupled to both a hot bath (its environment) with phonon occupancy \bar{n} and a coupling rate Γ , and a cold bath (the optical field). We showed in Section 4.2.1 that, if the optical driving field is in a coherent state, the effective phonon occupancy of the cold bath approaches zero (see Eq. (4.20)) in the well-resolved sideband regime ($\kappa \ll \Omega$). All that remains

¹⁰Note that we use the term "passive radiation pressure cooling" here to distinguish this work from feedback cooling where the position of the mechanical oscillator is measured and active feedback forces are then applied to the mechanical oscillator. Feedback cooling is introduced in Chapter 5.

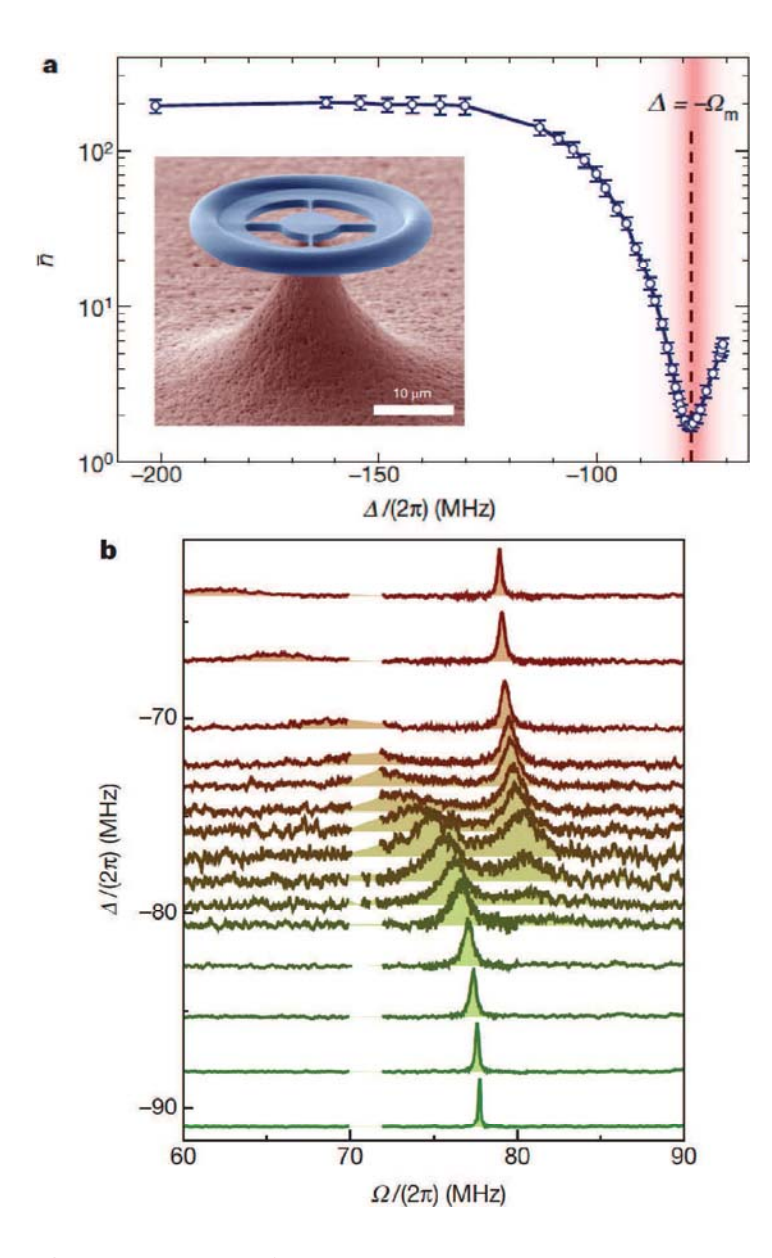


FIGURE 4.6 Observation of optomechanical cooling and quantumcoherent coupling. Adapted by permission from Macmillan Publishers Ltd: Nature [295], copyright 2012. Note that here $\Omega_{\rm m}$ and Ω respectively denote the mechanical resonance and optical sideband frequencies. (a) Mechanical occupancy (termed \bar{n} here) as a function of detuning Δ (our $-\Delta$). Inset: microtoroidal optomechanical system. (b) Mechanical power spectral density observed on output optical field showing the avoided crossing characteristic of strong coupling. The dip at exactly $\Delta = -\Omega$ shown in Fig. 4.4 for strong hybridisation is not observed here because the optical field probes the mechanical position spectral density, rather than the phonon number power spectral density.

to determine the occupancy of the mechanical oscillator in the well-resolved sideband regime is to determine the coupling rate between the mechanical oscillator and the optical bath. As we showed in Sections 4.2.2.1 and 4.2.2.2, this coupling rate is different in the weak and strong coupling regimes, with the optical cavity decay rate introducing a bottle-neck in the latter case.

Let us first consider the weak coupling regime, where the heat introduced to the intracavity optical field from the mechanical oscillator decays out of the cavity sufficiently fast to prevent the possibility of reheating the mechanics. In this regime, we can determine the coupling rate of the mechanical excitation into the optical cold bath by inspection of $\chi_{bb}(\delta)$. We found in Section 4.2.2.1 that, in the weak coupling regime, this is well approximated by the Lorenzian given in Eq. (4.36). We can immediately see from this expression that the effect of the optical field is to introduce a second decay channel with decay rate

$$\Gamma_{\text{opt}} = \frac{4g^2}{\kappa}.\tag{4.45}$$

It is worth commenting that this rate is identical to the rate $\mu = 4g^2/\kappa$ that information about the mechanical position is encoded on the output optical field in the nonresolved sideband limit which we identified in Section 3.3. Using this rate, along with the other parameters defined above, in Eq. (4.23) we exactly reproduce Eq. (4.39) for \bar{n}_b from Section 4.2.2.1 in the well sideband resolved weak coupling regime.

In Section 4.2.2.2 we found that, in the strong coupling regime, the coupling rate between the mechanical oscillator and the optical bath is

$$\Gamma_{\text{opt}} = \kappa.$$
 (4.46)

This can be understood since, in this regime, energy is exchanged back and forth between the cavity field and the mechanical oscillator until it eventually decays out of the cavity into the optical environment at rate κ . Using this rate in Eq. (4.23), we immediately retrieve the same steady-state occupancy as we derived in Section 4.2.2.2 (Eq. (4.43)).

4.3 OPTOMECHANICALLY INDUCED TRANSPARENCY

We have now seen how red detuning of the optical drive field to an optome-chanical system can enable mechanical cooling. More complicated protocols are possible by using multiple optical drive fields. Optomechanically induced transparency is one prominent example [4, 309, 246]. Optomechanically induced transparency is analogous to electromagnetically induced transparency (EIT), which allows the absorption spectrum and dispersion of ensembles of atoms to be engineered and is an important tool for quantum memories and repeaters [104]. Just as in EIT, in optomechanically induced transparency two laser fields are injected into the optical cavity, a weak probe field at a frequency near the optical resonance frequency, and a strong control field. The control field is red detuned by the mechanical frequency in the same manner as the

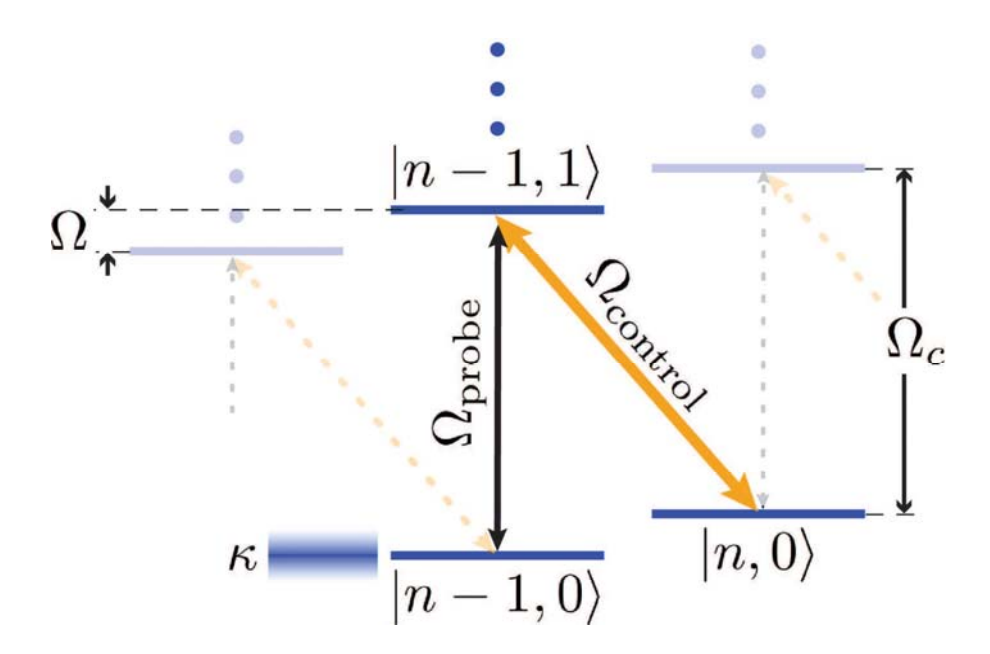


FIGURE 4.7 Energy level diagram for optomechanically induced transparency showing the control and probe optical tones at frequencies $\Omega_{\rm control}$ and $\Omega_{\rm probe}$, respectively. Similarly to Fig. 4.1 for optomechanical cooling, $|n,m\rangle$ represents an n-phonon, m-photon state.

cooling field in resolved sideband cooling. This pump-probe scheme is illustrated in the energy level diagram shown in Fig. 4.7 and allows a similar level of control over the absorption and dispersion of optical fields as EIT.

4.3.1 Hamiltonian

It is most convenient to solve for the dynamics of optomechanically induced transparency in the interaction picture at the cavity resonance frequency, such that $\Delta = 0$. Starting with the standard general optomechanical Hamiltonian of Eq. (2.18) within a rotating frame for the optical field, we then have

$$\hat{H} = \hbar \Omega b^{\dagger} b + \hbar q_0 a^{\dagger} a \left(b^{\dagger} + b \right). \tag{4.47}$$

Treating the control field as classical and much brighter than the probe field, this Hamiltonian may be linearised using a similar approach to that which we followed in Section 2.7.

We begin by reexpressing the annihilation operator a as

$$a \to a + \alpha e^{i\Omega t},$$
 (4.48)

where the first term constitutes the quantum fluctuations and any coherent contribution from the probe field, 11 while the second term represents the co-

¹¹Which must be small compared with α .

herent control tone which, in the same manner as the drive tone in resolved sideband cooling treated earlier, is red detuned from the cavity by the mechanical resonance frequency Ω . The term $a^{\dagger}a$ in the Hamiltonian (Eq. (4.47)) can then be expanded as

$$a^{\dagger}a \rightarrow \alpha^2 + a^{\dagger}a + \alpha \left[a^{\dagger}e^{i\Omega t} + ae^{-i\Omega t}\right]$$
 (4.49)

$$\approx \alpha \left[a^{\dagger} e^{i\Omega t} + a e^{-i\Omega t} \right]. \tag{4.50}$$

Here we have neglected the constant α^2 term, which, as we saw in Section 2.7, introduces a constant term in the Hamiltonian as well as a static displacement to the mechanical oscillator that has no effect on the dynamics of the system. We have also neglected the $a^{\dagger}a$ term in the usual linearisation approximation, with the probe field and vacuum optomechanical coupling rate g_0 assumed to be sufficiently weak so that this term does not appreciably affect the system dynamics. Substituting this expression into the Hamiltonian, we arrive at

$$\hat{H} = \hbar \Omega b^{\dagger} b + \hbar g \left[a^{\dagger} e^{i\Omega t} + a e^{-i\Omega t} \right] \left(b^{\dagger} + b \right) \tag{4.51}$$

$$\approx \hbar\Omega b^{\dagger} b + \hbar g \left[a b^{\dagger} e^{-i\Omega t} + a^{\dagger} b e^{i\Omega t} \right], \tag{4.52}$$

where, similar to our previous treatment of resolved sideband cooling, in the approximation we have neglected terms that are not resonant and are therefore suppressed in the resolved sideband limit (see Fig. 4.7). Apart from the explicit time dependence, this Hamiltonian is very similar to the Hamiltonian for resolved sideband cooling given in Eq. (4.27). The oscillation in time is crucial for the operation of optomechanically induced transparency and can be thought of experimentally as a beating between the probe and control fields that causes near DC fluctuations in the probe to be mixed up to the mechanical resonance frequency and thereby to strongly interact with the mechanical oscillator. In optomechanically induced transparency probe excitations are converted to mechanical oscillations and then back into the probe field again. The essential idea is to set up a perfect destructive interference between the intracavity probe field and the fluctuations it drives onto the mechanics when they return to the cavity. Thereby, the probe field cannot exist in the cavity, and the cavity becomes transparent.

4.3.2 Optomechanically induced absorption

We begin our treatment of optomechanically induced transparency by considering the open system dynamics of a single-sided optomechanical system – that is, one that has only a single optical input/output channel (see Fig. 4.8 (left)). This turns out to enable optomechanically induced absorption but not transparency. In Section 4.3.3, we will extend the treatment to a double-sided optomechanical system which does exhibit transparency. Similar to our approach to resolved sideband cooling in Section 4.2.2, within the regime of validity of the rotating wave approximation Eq. (1.112) may be used to obtain the equa-

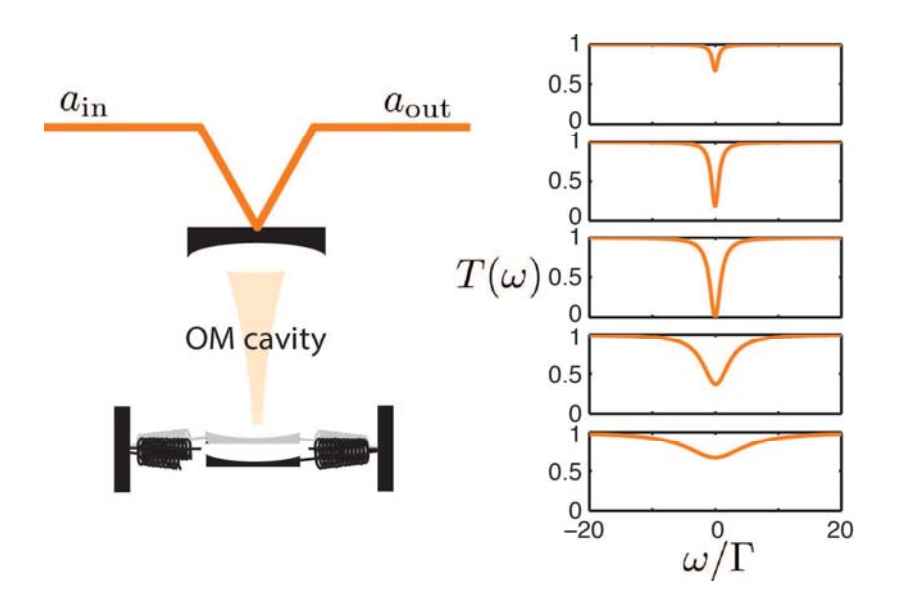


FIGURE 4.8 Optomechanically induced absorption in a single-sided optomechanical system. Left: Experimental schematic. Right: Modelled transmissivity $T(\omega)$ as a function of frequency ω for optomechanical cooperativities of $C = \{0.1, 0.4, 1, 4, 10\}$ from top to bottom, and $\kappa = 10\Gamma$.

tions of motion

$$\dot{a} = -\frac{\kappa}{2}a - igbe^{i\Omega t} + \sqrt{\kappa}a_{\rm in}$$
 (4.53)

$$\dot{b} = -\frac{\Gamma}{2}b - i\Omega b - igae^{-i\Omega t} + \sqrt{\Gamma}b_{\rm in}$$
 (4.54)

for the intracavity optical field and mechanical oscillator.

Exercise 4.11 Solve these equations of motion in the frequency domain to show that in the steady state

$$a(\omega) = \chi_{aa}(\omega)a_{\rm in}(\omega) + \chi_{ab}(\omega)b_{\rm in}(\omega + \Omega), \tag{4.55}$$

where $\chi_{aa}(\omega)$ and $\chi_{ab}(\omega)$ are the light-to-light and mechanical oscillator-to-light susceptibilities

$$\chi_{aa}(\omega) = \sqrt{\kappa} \left[\frac{\kappa}{2} - i\omega + \frac{g^2}{\Gamma/2 - i\omega} \right]^{-1}$$
 (4.56a)

$$\chi_{ab}(\omega) = -\sqrt{\Gamma} \left(\frac{ig}{\Gamma/2 - i\omega} \right) \left[\frac{\kappa}{2} - i\omega + \frac{g^2}{\Gamma/2 - i\omega} \right]^{-1}. \quad (4.56b)$$

As can be seen, the light-to-light susceptibility is modified from the usual Lorentzian describing a bare optical resonance, whilst the presence of the mechanical oscillator introduces a second input noise term in the equation, driving the intracavity optical field.

4.3.2.1 Output field

The output field from the system can be found using the general input-output relation of Eq. (1.125) with the result

$$a_{\text{out}} = t(\omega)a_{\text{in}}(\omega) + l(\omega)b_{\text{in}}(\omega + \Omega),$$
 (4.57)

where

$$t(\omega) = 1 - \sqrt{\kappa} \chi_{aa}(\omega) \tag{4.58a}$$

$$l(\omega) = -\sqrt{\kappa} \chi_{ab}(\omega). \tag{4.58b}$$

Here $t(\omega)$ is a complex frequency-dependent transmission coefficient that quantifies the fraction of the incident field that remains in the output field of the optomechanical system, while $l(\omega)$ quantifies the fraction of the mechanical bath fluctuations that are imprinted onto the output field. As we found in Section 4.2.2, in the resolved sideband regime with a strong drive field that is red detuned to $\Delta = \Omega$, the optomechanical interaction is of the form of a beam splitter, or equivalently a two-mode linear scattering interaction. From this perspective $t(\omega)$ and $l(\omega)$ can be thought of as scattering amplitudes, with $l(\omega)$ not only quantifying the level of mechanical fluctuations imprinted on the output field, but also the loss (or absorption) of the optical field by the mechanical bath – i.e., it is a frequency-dependent loss coefficient.

Exercise 4.12 Show that the optomechanical scattering process is energy conserving, with

$$T(\omega) + L(\omega) = 1, (4.59)$$

where the transmissivity $T(\omega)$ and absorptivity $L(\omega)$ are defined as $T(\omega) \equiv |t(\omega)|^2$ and $L(\omega) \equiv |l(\omega)|^2$. Show that, in the limit $\omega \ll \kappa$, the absorptivity is given by the Lorentzian

$$L(\omega) = \frac{C\Gamma^2}{(1+C)^2(\Gamma/2)^2 + \omega^2},$$
(4.60)

where, as usual, $C = 4g^2/\kappa\Gamma$ is the optomechanical cooperativity.

As the above exercise demonstrates, in this configuration the optomechanical system is acting as an optical absorber, with peak absorption at sideband frequencies that are close to Ω higher than the coherent drive frequency (i.e., near $\omega=0$). In the previous section we examined the effect of the optical field on the mechanical oscillator when a red-detuned coherent drive tone is applied, showing that cooling occurs due to (cold) optical fluctuations being transferred onto the oscillator. Here we see the complimentary effect on the optical field from the same process, with the mechanical oscillator absorbing optical energy. The absorptive feature is Lorenzian with a width $(1+C)\Gamma$ matching the optomechanically broadened mechanical linewidth of resolved

sideband cooling in the weak coupling regime (Eq. (4.38)), and exhibits a peak absorption of $4C/(1+C)^2$ when $\omega=0$.

The transmissivity $T(\omega)$ of this optomechanical absorber is plotted as a function of frequency in Fig. 4.8 (right) for a range of optomechanical cooperativities. One observation that can be made from this figure is that, in the special case of C=1, the optical field is perfectly absorbed by the mechanical oscillator at $\omega = 0$. Note that this does not imply that this choice of cooperativity allows the mechanical oscillator to be cooled to its ground state. As we saw in the previous section, significantly more stringent requirements must be satisfied to achieve this (see Eq. 4.44).

4.3.3 Optomechanically induced transparency using a double-sided optical cavity

In the case of a single-sided cavity considered in the previous section, when there is no optomechanical interaction (q = C = 0) energy conservation requires that the transmissivity $T(\omega) = 1$ for all sideband frequencies.

Exercise 4.13 Confirm that this is the case from Eq. (4.58a).

Consequently, in this single-sided configuration it is clearly not possible for the optomechanical interaction to enhance the transmissivity as required for optomechanically induced transparency. This motivates us to consider the case of a double-sided cavity as depicted in Fig. 4.9 (left). We envision that the cavity decay occurs through two optical ports with decay rates of κ_1 and κ_2 , respectively, though one of these ports may in fact arise due to optical losses and therefore not be readily accessible to the experimenter. The total cavity decay rate is then $\kappa = \kappa_1 + \kappa_2$. While the broad features of optomechanically induced transparency are evident for any choice of decay rates, we choose to consider a balanced two-sided cavity here, with $\kappa_1 = \kappa_2 = \kappa/2$. This has the advantage that, without optomechanical interaction, the optical field is fully impedance matched into the cavity through one input/output port, and out through the other input/output port.

For a balanced two-sided cavity, the input optical field of Eq. (4.57) has equal contributions from both optical ports so that

$$a_{\rm in} = \frac{a_{\rm in,1} + a_{\rm in,2}}{\sqrt{2}}. (4.61)$$

Exercise 4.14 Substituting this into Eq. (4.55) and using the input-output relations of Eq. (1.125), show that the two output fields are

$$a_{1,\text{out}} = t(\omega)a_{1,\text{in}}(\omega) + r(\omega)a_{2,\text{in}}(\omega) + l(\omega)b_{\text{in}}(\omega + \Omega)$$
 (4.62a)

$$a_{2,\text{out}} = t(\omega)a_{2,\text{in}}(\omega) + r(\omega)a_{1,\text{in}}(\omega) + l(\omega)b_{\text{in}}(\omega + \Omega), \qquad (4.62b)$$

where now

$$t(\omega) = 1 - \frac{\sqrt{\kappa}}{2} \chi_{aa}(\omega) \tag{4.63a}$$

$$r(\omega) = -\frac{\sqrt{\kappa}}{2} \chi_{aa}(\omega)$$
 (4.63b)

$$l(\omega) = -\sqrt{\frac{\kappa}{2}} \chi_{ab}(\omega), \qquad (4.63c)$$

with $r(\omega)$ being a complex frequency-dependent reflection coefficient describing the coupling from one optical field to the other.

Confirm that, analogously to the case of a single-sided optical cavity, energy is conserved with

$$T(\omega) + R(\omega) + L(\omega) = 1, \tag{4.64}$$

where the reflectivity $R(\omega)$ is defined as $R(\omega) \equiv |r(\omega)|^2$.

In the limit $\omega \ll \kappa$ the transmissivity $T(\omega)$ of this two-sided optomechanical system is well approximated by the Lorenzian

$$T(\omega) = \frac{C^2(\Gamma/2)^2}{(1+C)^2(\Gamma/2)^2 + \omega^2},$$
(4.65)

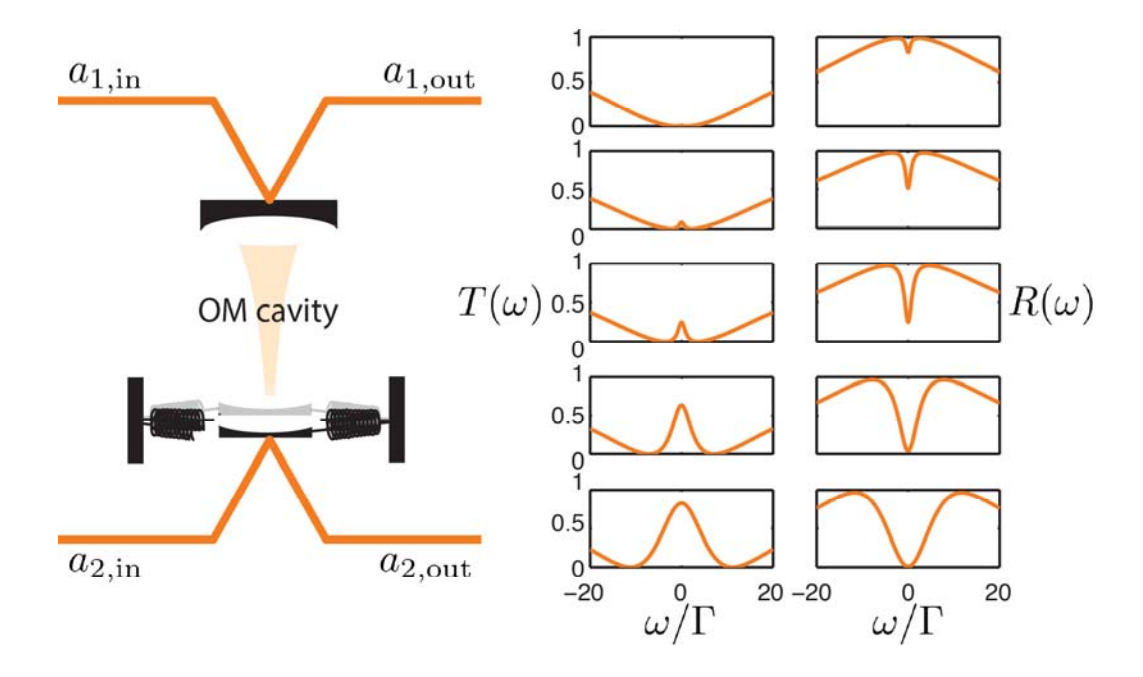


FIGURE 4.9 Optomechanically induced transparency in a double-sided optomechanical system. Left: Experimental schematic. Right: Modelled transmissivity $T(\omega)$ (left column) and reflectivity $R(\omega)$ (right column) as a function of frequency ω for optomechanical cooperativities of $C = \{0.1, 0.4, 1, 4, 10\}$ from top to bottom, and $\kappa = 50\Gamma$.

which is quite similar in form to the absorption spectrum in the single-sided case (Eq. (4.60)). We see that, when there is no optomechanical interaction (C=0), the optomechanical system has no on-resonance $(\omega=0)$ transmission. As the interaction strength increases, a transparency window now appears with peak transmissivity of $T(0) = C^2/(1+C)^2$ and width equal to the resolved sideband cooled mechanical linewidth $(1+C)\Gamma$. Asymptotically, at $C \to \infty$ the on-resonance transmissivity approaches unity; while at C=1 the optomechanical system acts as a balanced but lossy beam splitter with T(0)=R(0)=1/4 and L(0)=1/2. This behaviour is shown in Fig. 4.9 (right).

4.3.3.1 Noise performance

From the above observations it should now be clear that, in the linearised regime with coherent driving on the red sideband, a cavity optomechanical system acts as a tuneable beam splitter between the incident optical cavity fields and the mechanical bath fluctuations, with a sharp spectral response dependent on the mechanical decay rate and optomechanical cooperativity. It is interesting to ask what conditions are required for the fluctuations introduced by the mechanical oscillator to be negligible, such that the oscillator acts only as a sort of controllable noise-free valve connecting the two fields. Assuming that the input optical fields are both in coherent states and the mechanical bath is, as usual, in a thermal state with occupancy \bar{n} , the power spectral density of an arbitrary quadrature $\hat{X}_{1,\text{out}}^{\theta}$ of output field 1 can be easily shown using Eqs. (1.43), (1.118a), and (4.62) to be

$$S_{X_{1,\text{out}}^{\theta}X_{1,\text{out}}^{\theta}}(\omega) = \frac{T(\omega)}{2} + \frac{R(\omega)}{2} + L(\omega)(\bar{n} + 1/2),$$
 (4.66)

with an identical result for output field 2, where we have neglected the coherent peak from each optical field at $\omega = 0$. Making use of Eq. (4.64) we find the condition on the absorptivity

$$L(\omega) < \frac{1/2}{\bar{n}+1} \tag{4.67}$$

for the first two (optical) terms to dominate the last (mechanical) term. This regime can be achieved in both the high and low cooperativity limits. In the more interesting high cooperativity limit $(C \gg 1)$, for instance, the onresonance absorptivity is L(0) = 2/C and the condition becomes $C > 4(\bar{n}+1)$, which is a similar criterion as that to achieve ground state cooling in the weak coupling sideband-resolved regime (second inequality in Eq. (4.44)). If this condition is satisfied, the effect of the optomechanical interaction is to modify the optical susceptibility, creating a sharp transparency feature that – at least on-resonance – switches the output optical fields of the system without adding any appreciable fluctuations from the mechanical bath.

While the treatment in this section is only valid in the linearised regime, we

introduce single-photon optomechanical beam splitters which operate in the nonlinearisable single-photon strong coupling regime in Sections 6.3 and 6.4.

4.3.3.2 Experimental implementation

Optomechanically induced transparency has been experimentally demonstrated in a range of different architectures. It was first achieved in a microtoroidal optomechanical system [309]. Figure 4.10 shows the experimental apparatus, the overused transparency window, and resulting broadening and deepening of the transparency as a function of optomechanical cooperativity. One particularly remarkable feature of optomechanically induced transparency is demonstrated here. While a typical microcavity might have a resonance linewidth of megahertz or gigahertz, a typical micromechanical oscillator has a linewidth in the range of millihertz to kilahertz. The optomechanical transparency allows these ultra narrow linewidths to be mapped onto an optical field (see the exceptionally sharp transparency feature in Fig. 4.10b). One proposed application of such a sharp resonance is to apply a strongly frequency dependent rotation to squeezed light so that it can be used to exceed the standard quantum limit of the measurement of mechanical motion over a broad frequency band [185, 233] (we discuss this concept further in Section 5.4.2). It has proved practically difficult to achieve such rotations through other means.

4.4 OPTOMECHANICAL ENTANGLEMENT

In the previous two sections we considered the scenario where the optical field was red detuned from the optical resonance frequency, showing that this results in cooling of the mechanical oscillator and can be used to facilitate an optomechanically induced transparency for the optical field. It is interesting to consider the opposite regime where the optical field is blue detuned. Here, each incident photon carries more energy than an intracavity photon. When photons enter the cavity, the additional energy is taken up by the mechanical oscillator. One might initially imagine that this process would be undesirable, acting only to heat the mechanical oscillator. However, this is not the case. In fact it acts to correlate the intracavity field and the mechanical oscillator and ultimately generate entanglement between them, which is the topic of this section.

A wide range of theoretical studies have been performed on optome-chanical entanglement, with some of the earlier seminal works including [35, 188, 333, 299, 301, 116]. It was first experimentally demonstrated for a lumped element superconducting microwave optomechanical system in 2013 [217] (see Fig. 4.16).

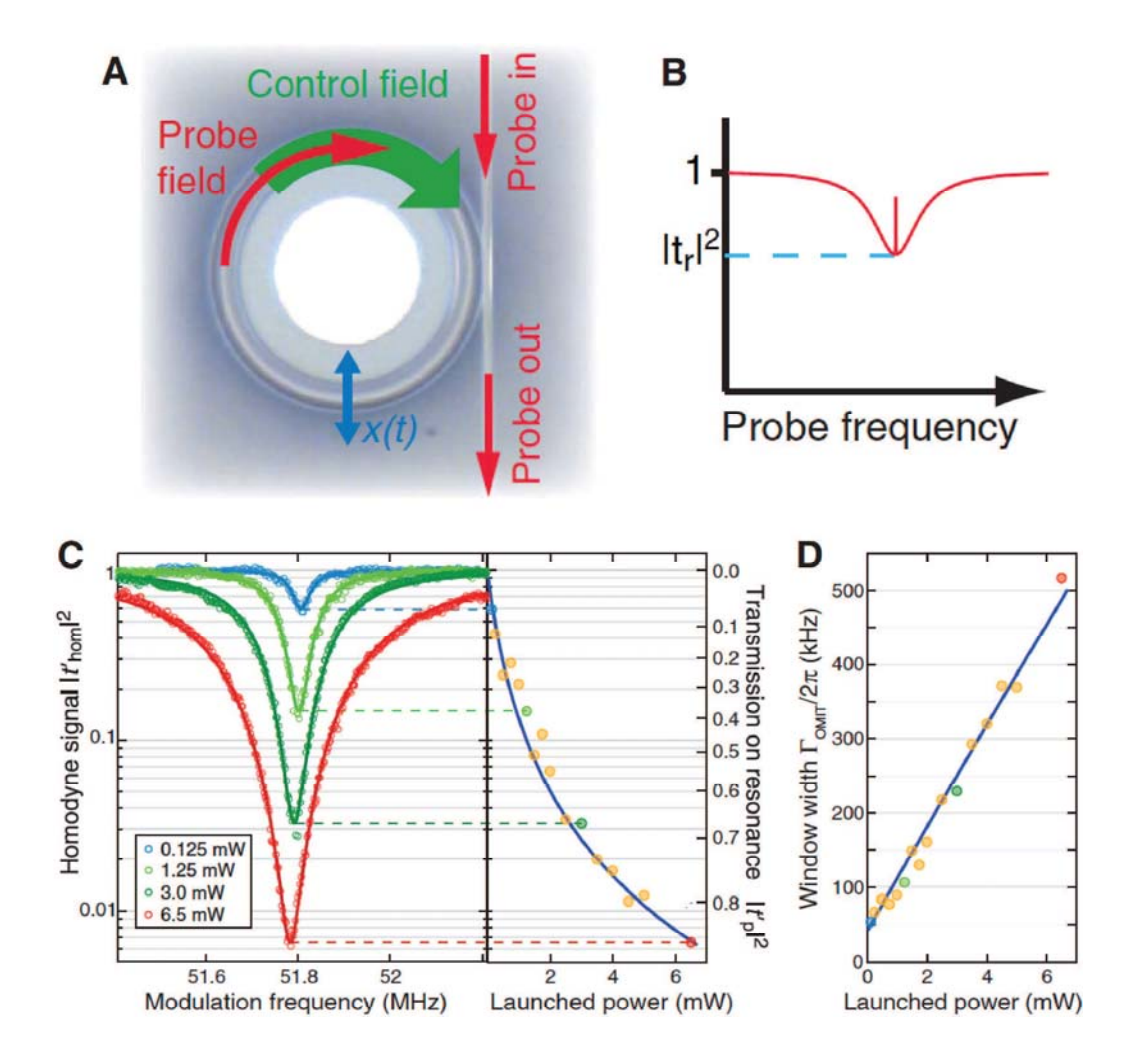


FIGURE 4.10 Experimental demonstration of optomechanically induced transparency. From [309]. Reprinted with permission from AAAS. (a) Microtoroidal optomechanical system showing probe and control fields. (b) Theoretical model of probe transmission as a function of frequency. (c) Observed homodyne signal showing a sharp dip near the mechanical resonance frequency, which in this configuration is evidence of an increased probe transmission at that frequency. (d) Width of transparency window as a function of laser power.

4.4.1 Hamiltonian and equations of motion

Similarly to our treatment of resolved sideband cooling in Section 4.2.2, for simplicity we consider the resolved sideband limit where $\kappa \ll \Omega$. In Section 4.2.2, this limit allowed us to apply a rotating wave approximation and neglect the off-resonant ab and $a^{\dagger}b^{\dagger}$ terms in the Hamiltonian of Eq. (4.1), resulting in a beam splitter-like Hamiltonian between a and b. Here we choose a blue detuning of $\Delta = -\Omega$ rather than red detuning, so that these terms are resonant (consider the energy level diagram in Fig. 4.1), and the ab^{\dagger} and $a^{\dagger}b$ terms are off-resonant. Neglecting the off-resonant terms, in an interaction picture with the optical field and mechanical oscillator rotating at the cavity and mechanical resonance frequencies, respectively, the optomechanical Hamiltonian of Eq. (4.1) then becomes

$$\hat{H} = \hbar g \left(ab + a^{\dagger} b^{\dagger} \right). \tag{4.68}$$

The effect of this Hamiltonian is immediately apparent – it is the Hamiltonian of a parametric interaction that generates (or annihilates) correlated photon-phonon pairs. It may appear that pair production of this kind would violate energy conservation. Indeed, unlike the case of a beam splitter, this Hamiltonian is not energy conserving in its own right, with the energy required to generate photon-phonon pairs derived from the coherent optical drive field. Parametric processes are the fundamental processes behind all forms of bipartite Gaussian entanglement. The ability to tune between beam splitter and parametric interactions via detuning is a particularly useful tool to control the physics of optomechanical systems.

The rotating wave quantum Langevin equation of Eq. (1.112) can be used, as usual, to arrive at equations of motion for the evolution of the intracavity field and mechanical oscillator:

$$\dot{a} = igb^{\dagger} - \frac{\kappa}{2}a + \sqrt{\kappa}a_{\rm in} \tag{4.69a}$$

$$\dot{b} = iga^{\dagger} - \frac{\Gamma}{2}b + \sqrt{\Gamma}b_{\rm in}. \tag{4.69b}$$

4.4.2 Bogoliubov modes

While the equations of motion in Eq. (4.69) can be straightforwardly solved by taking the Fourier transform and solving simultaneously, it is instructive to instead first diagonalise them.

Exercise 4.15 Show that substitution of a and b in terms of

$$c^{-} = \frac{1}{\sqrt{2}} \left(ira + \frac{1}{r} b^{\dagger} \right) \tag{4.70a}$$

$$c^{+} = \frac{1}{\sqrt{2}} \left(\frac{1}{r} a + irb^{\dagger} \right) \tag{4.70b}$$

diagonalises Eqs. (4.69), with the resulting uncoupled equations of motion given by

$$\dot{c}^{-} = -\frac{\gamma^{-}}{2}c^{-} + ir\sqrt{\frac{\kappa}{2}}a_{\rm in} + \frac{1}{r}\sqrt{\frac{\Gamma}{2}}b_{\rm in}^{\dagger}$$
 (4.71a)

$$\dot{c}^{+} = -\frac{\gamma^{+}}{2}c^{+} + \frac{1}{r}\sqrt{\frac{\kappa}{2}}a_{\rm in} + ir\sqrt{\frac{\Gamma}{2}}b_{\rm in}^{\dagger},$$
 (4.71b)

with

$$r = \frac{1}{\sqrt{2g}} \left[\frac{\kappa - \Gamma}{2} + \sqrt{\left(\frac{\kappa - \Gamma}{2}\right)^2 + 4g^2} \right]^{1/2}$$
 (4.72a)

$$\gamma^{\pm} = \frac{\kappa + \Gamma}{2} \mp \sqrt{\left(\frac{\kappa - \Gamma}{2}\right)^2 + 4g^2}.$$
(4.72b)

This transformation to modes c^{\pm} is a form of two-mode *Bogoliubov transformation*, used by Nickolai Bogoliubov to study the physics of superfluity and superconductivity [34]. Note that here c^{\pm} are not bosonic modes. From Eqs. (4.70) we find that c^{\pm} and c^{\mp} do not commute with each other:

$$\left[c^{\pm}, c^{\mp\dagger}\right] = \pm i,\tag{4.73}$$

while

$$\left[c^{\pm}, c^{\pm\dagger}\right] = \pm \frac{1}{2} \left(\frac{1}{r^2} - r^2\right).$$
 (4.74)

It is apparent from this second commutation relation that each operator commutes with its own conjugate for the special case of r=1, so that, for any arbitrary functions f and h, $[f(c^{\pm}, c^{\pm \dagger}), h(c^{\pm}, c^{\pm \dagger})] = 0$. We therefore see that, unlike the usual boson annihilation and creation operators, for r=1 there exists no Heisenberg uncertainty principle between the quadratures

$$\hat{X}_{c}^{-} \equiv \frac{1}{\sqrt{2}} \left(c^{-\dagger} + c^{-} \right) \stackrel{r=1}{=} \frac{1}{\sqrt{2}} \left(\hat{X}_{M} - \hat{Y}_{L} \right)$$
 (4.75a)

$$\hat{Y}_c^- \equiv \frac{i}{\sqrt{2}} \left(c^{-\dagger} - c^- \right) \stackrel{r=1}{=} \frac{1}{\sqrt{2}} \left(\hat{X}_L - \hat{Y}_M \right), \tag{4.75b}$$

where \hat{X}_M and \hat{Y}_M are mechanical quadrature operators (see Eqs. (1.135)) rotating at the mechanical resonance frequency Ω , which we term the mechanical position quadrature and the mechanical momentum quadrature, respectively, ¹² and we have introduced the subscript L to clearly distinguish the quadratures of the intracavity optical field from those of the mechanical oscillator.

Exercise 4.16 Determine the equivalent of Eqs. (4.75) for the quadratures $\hat{X}_c^+ \equiv (c^{+\dagger} + c^+)/\sqrt{2}$ and $\hat{Y}_c^+ \equiv i(c^{+\dagger} - c^+)/\sqrt{2}$.

We see from Eqs. (4.75) and the commutation relation $[\hat{X}_c^-, \hat{Y}_c^-] \stackrel{r=1}{=} 0$ that \hat{X}_M can in principle be perfectly correlated to \hat{Y}_L , while simultaneous perfect correlations exist between \hat{X}_L and \hat{Y}_M . This is the essential feature of two-mode Gaussian entanglement [237] and demonstrates the role that Bogoliubov modes play in understanding such entanglement.

¹²Note that the appearance of mechanical quadrature operators here, rather than the dimensionless position \hat{Q} and momentum \hat{P} , arises because – unlike our approach in previous parts of the textbook – in the Hamiltonian of Eq. (4.68) we have moved into an interaction picture for the mechanical oscillator rotating at Ω.

From Eq. (4.72b) it is apparent that each of the modes c^{\pm} decay at different rates that depend on κ , Γ , and g, with c^- (c^+) decaying faster (slower) than the mean of the optical and mechanical decay rates. Some straightforward algebra shows that γ^+ is negative for C>1 where, as usual, C is the optomechanical cooperativity. C=1 therefore constitutes a threshold for instability, above which c^+ grows exponentially as a result of the optomechanical interaction, never reaching a steady state. This is an example of parametric instability [159, 61]. While this exponential growth can, in principle, be stabilised – for instance, using feedback [134] or a secondary optical cooling tone [231] – or mitigated by using short optical pulses [217], here we restrict our analysis to the intrinsically stable regime where C<1.

4.4.3 Optical and mechanical modes in the stable regime

Taking the Fourier transform of Eqs. (4.71), we arrive at uncoupled equations of motion for $c^{\pm}(\omega)$ at steady state in the stable regime

$$c^{-}(\omega) = \left(\frac{1}{\gamma^{-}/2 - i\omega}\right) \left[ir\sqrt{\frac{\kappa}{2}} a_{\rm in}(\omega) + \frac{1}{r} \sqrt{\frac{\Gamma}{2}} b_{\rm in}^{\dagger}(-\omega) \right]$$
(4.76a)

$$c^{+}(\omega) = \left(\frac{1}{\gamma^{+}/2 - i\omega}\right) \left[\frac{1}{r}\sqrt{\frac{\kappa}{2}}\hat{a}_{\rm in}(\omega) + ir\sqrt{\frac{\Gamma}{2}}b_{\rm in}^{\dagger}(-\omega)\right]. \quad (4.76b)$$

Using Eqs. (4.70), the frequency domain annihilation operators for the intracavity optical field and mechanical oscillator can then be directly obtained. Expressed in terms of quadrature operators, they are

$$\hat{X}_L(\omega) = \chi_{aa}(\omega)\hat{X}_{L,\text{in}}(\omega) + \chi_{ab}(\omega)\hat{Y}_{M,\text{in}}(\omega)$$
 (4.77a)

$$\hat{Y}_L(\omega) = \chi_{aa}(\omega)\hat{Y}_{L,\text{in}}(\omega) + \chi_{ab}(\omega)\hat{X}_{M,\text{in}}(\omega)$$
 (4.77b)

$$\hat{X}_{M}(\omega) = \chi_{bb}(\omega)\hat{X}_{M,\text{in}}(\omega) + \chi_{ba}(\omega)\hat{Y}_{L,\text{in}}(\omega) \tag{4.77c}$$

$$\hat{Y}_{M}(\omega) = \chi_{bb}(\omega)\hat{Y}_{M,\text{in}}(\omega) + \chi_{ba}(\omega)\hat{X}_{L,\text{in}}(\omega), \qquad (4.77d)$$

where the susceptibilities $\chi_{ij}(\omega)$ are

$$\chi_{aa}(\omega) = \frac{\sqrt{\kappa} (\Gamma/2 - i\omega)}{(\kappa/2 - i\omega) (\Gamma/2 - i\omega) - g^2}$$
(4.78a)

$$\chi_{bb}(\omega) = \frac{\sqrt{\Gamma} (\kappa/2 - i\omega)}{(\kappa/2 - i\omega) (\Gamma/2 - i\omega) - q^2}$$
(4.78b)

$$\chi_{ab}(\omega) = \frac{g\sqrt{\Gamma}}{(\kappa/2 - i\omega)(\Gamma/2 - i\omega) - g^2}$$
(4.78c)

$$\chi_{ba}(\omega) = \frac{g\sqrt{\kappa}}{(\kappa/2 - i\omega)(\Gamma/2 - i\omega) - g^2}.$$
 (4.78d)

Exercise 4.17 Derive these expressions.

4.4.4 Einstein-Podolsky-Rosen entanglement

Gaussian two-mode entanglement, as produced by the linearised optomechanical interaction, was first considered by Einstein, Podolsky, and Rosen in 1935 [100]. They considered two quantum particles A and B described by the wave function

$$\psi_{AB}(x_A, x_B) = \int e^{ip(x_A - x_B)/\hbar} dp. \tag{4.79}$$

Since it is not possible to write this wave function in a product form $\psi_A(x_A)\,\psi_B(x_B)$, the state is inseparable and subsystems A and B are entangled. Einstein, Podolsky, and Rosen were particularly interested in the correlations exhibited between the particles with this wave function and the implications of these correlations on our understanding of quantum mechanics. They recognised that a perfect measurement of \hat{x}_A with result x_A will collapse the state of particle B into the position eigenstate $\psi_{B|A}(x_B) = \delta(x_A)$; while similarly, a perfect momentum measurement collapses particle B into the momentum eigenstate. Since subsystems A and B can in general be space-like separated, ¹³ the ability to predict both the position and momentum of particle B with perfect precision using different measurements on particle A introduces a conflict between quantum mechanics and local realism – either wave function collapse must occur faster than the speed of light or the position and momentum of particle B must exist with less indeterminism than required by the Heisenberg uncertainty principle. This apparent paradox is now referred to as the Einstein-Podolsky-Rosen paradox.

The perfect Einstein-Podolsky-Rosen state exhibits perfectly correlated position and momentum quadratures, such that

$$\left\langle \hat{X}_A(t) - \hat{Y}_B(t) \right\rangle = 0$$
 (4.80a)

$$\left\langle \hat{Y}_A(t) - \hat{X}_B(t) \right\rangle = 0,$$
 (4.80b)

where we have rotated the correlations compared to the previous paragraph such that they occur between position and momentum quadratures since, as we found in the previous section, this is the form of correlation generated by the optomechanical interaction. We see that, for a perfect Einstein-Podolsky-Rosen state, a noise-free measurement of the momentum quadrature of B collapses A into a position eigenstate, while similarly a noise-free measurement of the position quadrature of B collapses A into a momentum eigenstate.

By inspection of Eqs. (4.77), we can immediately observe that the optomechanical interaction produces correlations of a form similar to what would be expected for an ideal Einstein-Podolsky-Rosen state, but that the correla-

 $^{^{13}}$ While in the wave function of Eq. (4.79) the two particles are co-located, a separation s can be introduced straightforwardly via the modification $\psi_{AB}(x_A, x_B) =$ $\int e^{ip(x_A-x_B+s)/\hbar}dp$.

tions are imperfect. In the following two subsections, we introduce the standard methods to quantify two-mode Gaussian entanglement in the presence of such imperfections.

4.4.5 Covariance matrix

In the linearised regime considered here, the entanglement generated via the optomechanical interaction between light and a mechanical oscillator is a form of two-mode Gaussian entanglement. Two-mode Gaussian states are fully characterised by their quadrature expectation values and the covariance matrix

$$\mathbf{M} = \begin{bmatrix} V_{X_A X_A} & V_{X_A Y_A} & V_{X_A X_B} & V_{X_A Y_B} \\ V_{Y_A X_A} & V_{Y_A Y_A} & V_{Y_A X_B} & V_{Y_A Y_B} \\ V_{X_B X_A} & V_{X_B Y_A} & V_{X_B X_B} & V_{X_B Y_B} \\ V_{Y_B X_A} & V_{Y_B Y_A} & V_{Y_B X_B} & V_{Y_B Y_B} \end{bmatrix} = \begin{bmatrix} \mathbf{A} & \mathbf{C} \\ \mathbf{C}^T & \mathbf{B} \end{bmatrix}$$
(4.81)

where

$$V_{\mathcal{A}\mathcal{B}} \equiv \frac{\left\langle \hat{\mathcal{A}}(t)\hat{\mathcal{B}}(t)\right\rangle + \left\langle \hat{\mathcal{B}}(t)\hat{\mathcal{A}}(t)\right\rangle}{2} - \left\langle \hat{\mathcal{A}}(t)\right\rangle \left\langle \hat{\mathcal{B}}(t)\right\rangle \tag{4.82}$$

is the covariance between operators $\hat{\mathcal{A}}$ and $\hat{\mathcal{B}}$, the 2×2 matrices **A** and **B** quantify the variances of the optical and mechanical quadratures and the internal correlations within each subsystem, while **C** quantifies the correlations between the mechanical oscillator and the optical field.

4.4.6 Identifying and quantifying entanglement

Diagonalisation of the covariance matrix of Eq. (4.81) yields a pair of symplectic eigenvalues ν_{\pm} [256]. As first recognised simultaneously by Duan and Simon [97, 261], the condition

$$\nu_{-} < \frac{1}{2} \tag{4.83}$$

is necessary and sufficient for two-mode Gaussian entanglement, where ν_- is the smaller of the two eigenvalues. For a general covariance matrix, the symplectic eigenvalues are given by

$$\nu_{\pm} = \left[\frac{1}{2} \left(\tilde{\Delta} \pm \sqrt{\tilde{\Delta}^2 - 4 \det(\mathbf{M})} \right) \right]^{1/2}, \tag{4.84}$$

where det(...) is the determinant and

$$\tilde{\Delta} = \det(\mathbf{A}) + \det(\mathbf{B}) - 2\det(\mathbf{C}). \tag{4.85}$$

The significance of the smaller symplectic eigenvalue with regards to quantum correlations may be understood in the following way. Consider a pair of

collective observables of the subsystems A and B

$$\hat{u} = \hat{X}_A + c\hat{X}_B \tag{4.86a}$$

$$\hat{v} = \hat{Y}_A - c\hat{Y}_B, \tag{4.86b}$$

where c is a real constant. If subsystems A and B share no correlations, or indeed share only classical correlations introduced via local operations and classical communication, then the minimum possible product of standard deviations of \hat{u} and \hat{v} is easily shown to be

$$\min\left\{\sigma(\hat{u})\sigma(\hat{v})\right\}_{\text{uncor}} = \frac{1+c^2}{2},\tag{4.87}$$

and is achieved when both \hat{u} and \hat{v} are symmetric minimum uncertainty states, i.e., vacuum or coherent states.

Exercise 4.18 Convince yourself of this.

The criterion of Duan and Simon can be interpreted as stating that subsystems A and B are inseparable if-and-only-if there exists a choice of c for which arbitrary local operations on each individual subsystem are able to bring the product of standard deviations $\sigma(\hat{u})\sigma(\hat{v})$ beneath this value – i.e., if the joint uncertainty in \hat{u} and \hat{v} can be made smaller than the smallest possible uncertainty in the absence of quantum correlations. For a given inseparable state, the smaller symplectic eigenvalue ν_- quantifies exactly this ratio. Specifically,

$$\nu_{-} = \frac{1}{2} \min \left\{ \frac{\sigma(\hat{u})\sigma(\hat{v})}{\min \left\{ \sigma(\hat{u})\sigma(\hat{v}) \right\}_{\text{uncor}}} \right\} = \min \left\{ \frac{\sigma(\hat{u})\sigma(\hat{v})}{1 + c^2} \right\}, \tag{4.88}$$

where, here, the minimisation is taken over c and all possible local operations.¹⁴

The *logarithmic negativity* is a convenient and commonly used parameter to quantify the strength of a given entanglement resource and has the attractive properties of both being additive for multiple independent entangled states and quantifying the maximum distillable entanglement [229]. For two-mode Gaussian entangled states it is given by

$$L = \min\{0, -\log_2(2\nu_-)\}. \tag{4.89}$$

4.4.7 Entanglement between intracavity field and mechanical oscillator

Given the optomechanical covariance matrix, Eqs. (4.89) and (4.84) allow quantification of the entanglement between the intracavity optical field and

 $^{^{14}}$ Note that here we express the criterion of Duan in a product form as introduced in [36], rather than the more familiar sum form. The product form is in the spirit of the Heisenberg uncertainty relation or the criteria for the Einstein–Podolsky–Rosen paradox [237], and also achieves the minimum ν_{-} for a wider class of covariance matrices.

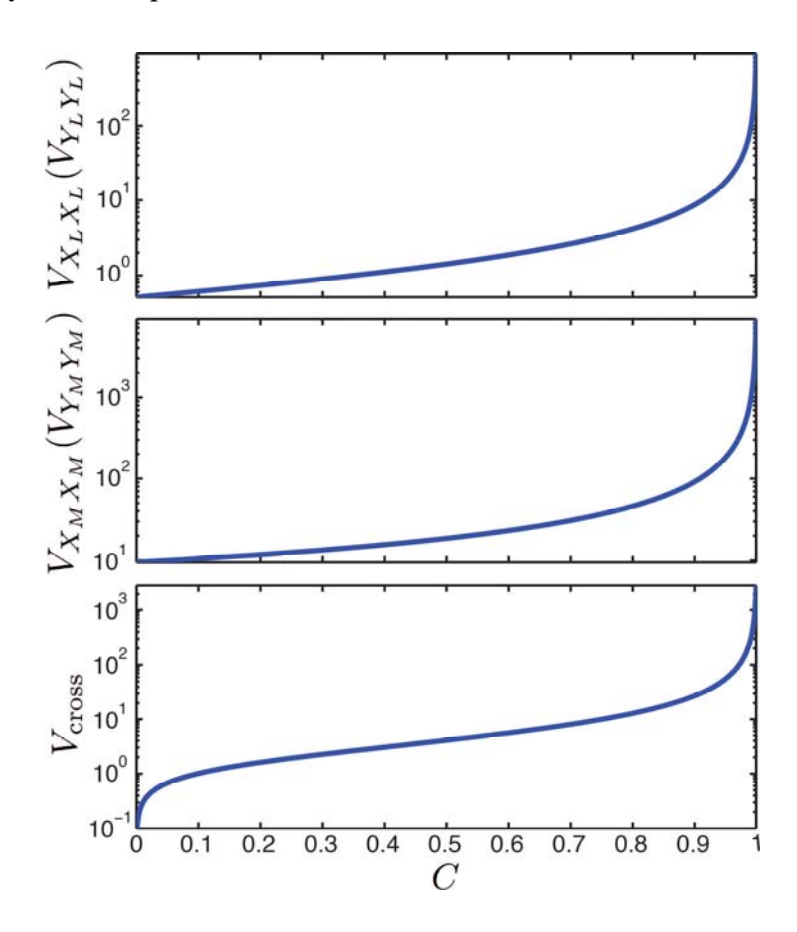


FIGURE 4.11 Covariance matrix elements of intracavity optomechanical entanglement as a function of optomechanical cooperativity C. Model parameters: $\bar{n} = 9$, $\bar{n}_L = 0.009$, $\kappa = 10 \Gamma$.

the mechanical oscillator. By inspection of Eqs. (4.77) we can immediately recognise that, as long as there are no correlations in the optical and mechanical baths, there will be no correlations between the amplitude and phase quadratures of the optical field, or indeed between the position and momentum quadratures of the mechanical oscillator, ¹⁵ so that

$$V_{X_L Y_L} = V_{Y_L X_L} = V_{X_M Y_M} = V_{Y_M X_M} = 0. (4.90)$$

Furthermore, the correlations between light and mechanics are all crossquadrature with

$$V_{X_L X_M} = V_{X_M X_L} = V_{Y_L Y_M} = V_{Y_M Y_L} = 0. (4.91)$$

Therefore, the only covariance matrix elements that must be determined are the variances $V_{X_LX_L}$, $V_{Y_LY_L}$, $V_{X_MX_M}$, and $V_{Y_MY_M}$, and the covariances

¹⁵This should be clear because the bath terms that appear in the equations for $\hat{X}_L(\omega)$ and $\hat{Y}_M(\omega)$ are different from those that appear in the equations for $\hat{Y}_L(\omega)$ and $\hat{X}_M(\omega)$.

 $V_{X_LY_M}$, $V_{Y_MX_L}$, $V_{Y_LX_M}$, and $V_{X_MY_L}$. For each of these elements the operators \mathcal{A} and \mathcal{B} in $V_{\mathcal{A}\mathcal{B}}$ commute. Furthermore, since the optomechanical Hamiltonian is linearised, $\langle \hat{X}_L \rangle = \langle \hat{Y}_L \rangle = \langle \hat{X}_M \rangle = \langle \hat{Y}_M \rangle = 0$ (see Section 2.7). These two properties allow the definition of the covariance matrix elements in Eq. (4.82) to be reexpressed more simply as

$$V_{\mathcal{A}\mathcal{B}} = \left\langle \hat{\mathcal{A}}(t)\hat{\mathcal{B}}(t) \right\rangle \tag{4.92}$$

$$= \frac{1}{2\pi} \int_{-\infty}^{\infty} d\omega \, S_{\mathcal{A}\mathcal{B}}(\omega) \tag{4.93}$$

$$= \frac{1}{2\pi} \iint_{-\infty}^{\infty} d\omega \, d\omega' \left\langle \hat{\mathcal{A}}^{\dagger}(-\omega) \hat{\mathcal{B}}(\omega') \right\rangle, \tag{4.94}$$

where to arrive at this result we have, as usual, used Parseval's theorem and the definition of the power spectral density in Eq. (1.43).

Exercise 4.19 Using Eqs. (4.77) and (4.94) show that the nonzero covariance matrix elements are

$$V_{X_L X_L} = V_{Y_L Y_L}$$

$$= \bar{n}_L + \frac{1}{2} + \left(\frac{C}{1 - C}\right) \left(\frac{1}{1 + \kappa/\Gamma}\right) (\bar{n}_L + \bar{n} + 1)$$
 (4.95a)

$$V_{X_M X_M} = V_{Y_M Y_M}$$

$$= \bar{n} + \frac{1}{2} + \left(\frac{C}{1 - C}\right) \left(\frac{1}{1 + \Gamma/\kappa}\right) (\bar{n}_L + \bar{n} + 1)$$
(4.95b)

$$V_{\text{cross}} = \left(\frac{\sqrt{C}}{1 - C}\right) \left(\frac{1}{\sqrt{\kappa/\Gamma} + \sqrt{\Gamma/\kappa}}\right) (\bar{n}_L + \bar{n} + 1)$$
 (4.95c)

where
$$V_{\text{cross}} = V_{X_L Y_M} = V_{Y_M X_L} = V_{X_M Y_L} = V_{Y_L X_M}$$
.

We see from Eqs. (4.95) that the variances of the optical field and mechanical oscillator are each equal to their respective bath variances plus a modification that depends on the optomechanical cooperativity C, the ratio of optical and mechanical decay rates, and the sum of the mechanical and optical bath variances; with cross-correlations growing from zero as the optomechanical cooperativity increases. The functional dependence of the variances and covariances on cooperativity are shown in Fig. 4.11. The equal magnitude of the two optical quadrature variances, as well as the two mechanical quadrature variances, and all of the cross-variances, is a result of limiting our treatment to high-quality oscillators for which it is possible to make a rotating wave approximation. In this regime any fast fluctuations that can cause differences between the variances are averaged out. It can also be observed that, as the system approaches instability $(C \to 1)$, all three correlation matrix elements approach infinity.

With the covariance matrix elements determined, the logarithmic negativity can be straightforwardly calculated using Eqs. (4.84) and (4.89). The

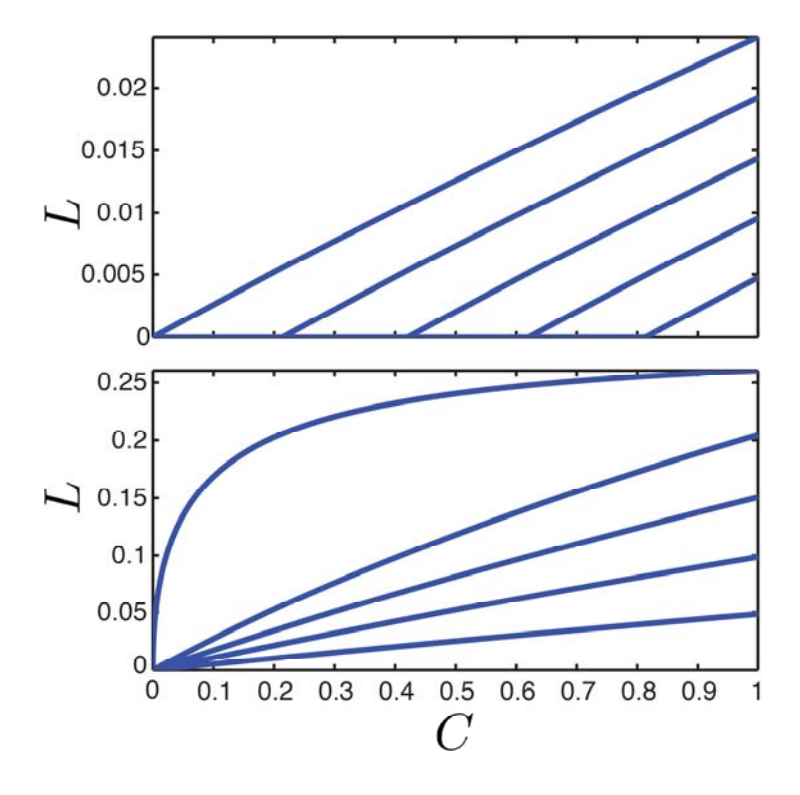


FIGURE 4.12 Logarithmic negativity of intracavity optomechanical entanglement as a function of optomechanical cooperativity C, with $\kappa = 10 \Gamma$. Top: Mechanical bath occupancy held fixed at $\bar{n} = 9$, with optical bath occupancy increasing over the range $\bar{n}_L = \{0, 0.002, 0.004, 0.006, 0.008\}$ from the top to bottom trace. Bottom: Optical bath occupancy held fixed at $\bar{n}_L = 0$, with mechanical bath occupancy increasing over the range $\bar{n} = \{0, 2, 4, 6, 8\}$ from the top to bottom trace.

resulting expressions are not, in general, particularly illuminating. Instead of reproducing them here, the logarithmic negativity is plotted as a function of optomechanical cooperativity for a range of different optical \bar{n}_L and mechanical \bar{n} bath occupancies and $\kappa/\Gamma=10$ in Fig. 4.12. We see that, in general, the entanglement improves as the cooperativity increases. From Fig. 4.12(top) it is clear that when the mechanical bath has nonzero occupancy, there is a threshold cooperativity beneath which no entanglement is present, with the threshold increasing as the optical bath occupancy increases. By contrast, Fig. 4.12(bottom) shows that, in the realistic scenario where the optical bath occupancy approaches zero, no such threshold is evident, with entanglement existing for any mechanical bath occupancy and any nonzero cooperativity. Indeed, this result can be shown to be true in general, so long as the optical decay is fast compared to the mechanical decoherence rate, specifically in circumstances where $\kappa > \bar{n}\Gamma$.

As the optomechanical cooperativity approaches the point of instability $(C \to 1)$, entanglement is present as long as

$$\left(\frac{\kappa}{\Gamma}\right)\bar{n}_L + \left(\frac{\Gamma}{\kappa}\right)\bar{n} < 1,\tag{4.96}$$

which restricts the optical and mechanical decoherence rates to be smaller than the mechanical and optical decay rates, respectively.

4.4.8 Entanglement of the mechanical oscillator with the external field

In the usual regime that $\kappa \gg \Gamma$, the interaction of the optomechanical system with the external optical field occurs much more rapidly than with the mechanical bath. While this interaction degrades the entanglement present between the intracavity optical field and the mechanical oscillator, since the output optical field is generally accessible experimentally, it is natural to ask how strongly it is entangled to the mechanical oscillator. Using the input-output relations of Eq. (1.125) and the intracavity field quadratures of Eqs. (4.77a) and (4.77b), the output field quadratures from the optomechanical system can be expressed in the frequency domain as

$$\hat{X}_{L,\text{out}}(\omega) = \left[1 - \sqrt{\kappa} \chi_{aa}(\omega)\right] \hat{X}_{L,\text{in}}(\omega) - \sqrt{\kappa} \chi_{ab}(\omega) \hat{Y}_{M,\text{in}}(\omega) \tag{4.97a}$$

$$\hat{Y}_{L,\text{out}}(\omega) = \left[1 - \sqrt{\kappa}\chi_{aa}(\omega)\right]\hat{Y}_{L,\text{in}}(\omega) - \sqrt{\kappa}\chi_{ab}(\omega)\hat{X}_{M,\text{in}}(\omega). \tag{4.97b}$$

As we saw in Section 1.4, in the Markov and rotating wave approximations the input and output fields of an optical cavity can be thought of as a train of infinitesimally separated infinitely narrow optical pulses. At any moment in time t the mechanical oscillator will exhibit entanglement with some ensemble of the output pulses, with the correlations decaying over a time scale that can be expected to depend in some way on the optical cavity and mechanical linewidths κ and Γ . Given this decay of correlations, there exists an optimal temporal mode for the output field that displays maximal correlations (and therefore entanglement) with the oscillator at time t. We would like to identify this optimal mode.

To approach this problem, we define a temporal mode of the output field with modeshape u(t), and annihilation operator

$$a_u(t) = u(t) * a_{\text{out}}(t), \tag{4.98}$$

where u(t) is normalised such that

$$\int_{-\infty}^{\infty} |u(t)|^2 dt = 1. \tag{4.99}$$

Exercise 4.20 Show that this normalisation of u(t) ensures that a_u obeys the usual Boson commutation relation

$$[a_u(t), a_u^{\dagger}(t)] = 1.$$
 (4.100)

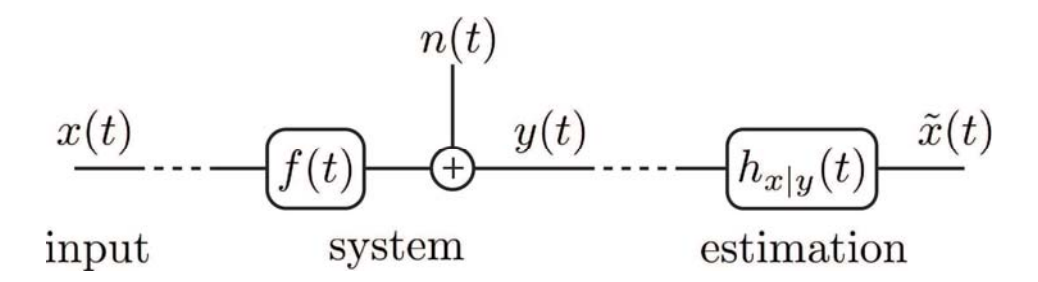


FIGURE 4.13 Schematic diagram of the use of classical Wiener filtering to estimate a continuous-in-time signal x(t) after it has been processed by a system that filters it (f(t)) and adds noise (n(t)). $\tilde{x}(t)$ is the final estimate.

The entanglement between this output temporal mode and the mechanical oscillator can be quantified in a manner similar to the case for the intracavity field dealt with in the previous section. However, as discussed already, before doing this we would like to determine the mode that exhibits maximal entanglement with the mechanical oscillator. This is the topic of the next section.

4.4.8.1 Wiener filtering

Estimation of a signal x(t) from a measurement y(t) is a common problem in classical control systems and information processing. For stationary processes and additive noise n(t), the measurement y(t) is related to the signal via y(t) = f(t) * x(t) + n(t), where f(t) is some filter function. In this scenario, the optimal estimation strategy is to apply a Wiener filter $h_{x|y}(t)$ to y(t), retrieving an estimate of the signal $\tilde{x}(t) = h_{x|y}(t) * y(t)$ (see Fig. 4.13) [311].

Since linear quantum systems such as that described by the linearised optomechanical Hamiltonian of Eq. (2.18) are unable to generate Wigner function negativity, their statistics may be fully explained through an equivalent classical process. As such, results from classical information processing can be readily applied [90]. In our specific case, Wiener filtering can be used to determine the optimal filter to apply to a measurement on the output field from a cavity optomechanical system to estimate the position quadrature (or momentum quadrature) of the mechanical oscillator at time t. As well as providing key information to practically perform measurement-based conditioning protocols such as feedback cooling as discussed in Chapter 5, this process identifies the temporal modes of the output field that are maximally correlated to each of the position and momentum quadratures of the mechanical oscillator at time t.

Both causal and noncausal Wiener filters exist [53]. Noncausal filters are generally used in information processing where one has access to the full measurement record, while causal filters are appropriate for real-time control ap-

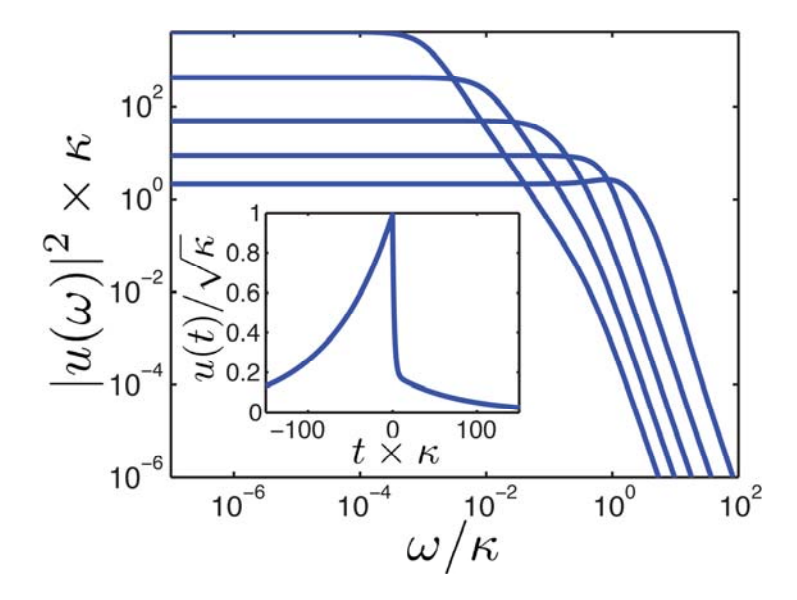


FIGURE 4.14 Wiener filter for optimal entanglement between a mechanical oscillator and an external optical field, with optomechanical cooperativity C = 0.9 and bath occupancies $\bar{n} = \bar{n}_L = 0$ and for $\kappa/\Gamma = \{0.1, 1, 10, 100, 1000\}$ from the bottom to the top trace. Inset, corresponding time-domain wave-packet for $\kappa = 100 \,\Gamma$. Note that these filters are noncausal.

plications where only the measurement record prior to the time t is available. In assessing optomechanical entanglement we should, in principle, use a causal filter since at time t the mechanical oscillator can only be entangled with the external optical field that has already interacted with it and has left the system before that time. However, for simplicity here we instead use a noncausal filter. 16 Once we have obtained solutions for the profile of the optimal noncausal temporal mode, we will be able to assess how close to causal they are. The exact noncausal Wiener filter is given in the frequency domain by [53]

$$h_{x|y}(\omega) = \frac{S_{yx}(\omega)}{S_{yy}(\omega)},\tag{4.101}$$

where $S_{yy}(\omega)$ and $S_{yx}(\omega)$ are the usual self- and cross-power spectral densities. As can be observed in Eqs. (4.97), only the mechanical momentum quadrature appears on the output optical amplitude quadrature; similarly, only the mechanical position quadrature appears on the output optical phase quadrature. The Wiener filters that allow optimal estimation of each mechanical

¹⁶The reader is encouraged to approach the same problem using causal filtering.

quadrature are then given by

$$h_{X_M|Y_{L,\text{out}}}(\omega) = \frac{S_{Y_{L,\text{out}}X_M}(\omega)}{S_{Y_{L,\text{out}}Y_{L,\text{out}}}(\omega)}$$
 (4.102a)

$$h_{Y_M|X_{L,\text{out}}}(\omega) = \frac{S_{X_{L,\text{out}}Y_M}(\omega)}{S_{X_{L,\text{out}}X_{L,\text{out}}}(\omega)}.$$
 (4.102b)

These filter functions are not identical, in general, which leads to some ambiguity as to the temporal mode that is maximally entangled to the mechanical oscillator. Here, however, since our analysis is limited to the regime in which the rotating wave approximation is valid, the filters coincide. Using Eqs. (4.97), they can be found to be

$$h(\omega) = \frac{(1 - \sqrt{\kappa} \chi_{aa}(\omega)) \chi_{ba}^{*}(\omega) (\bar{n}_{L} + 1/2) - \sqrt{\kappa} \chi_{ab}(\omega) \chi_{bb}^{*}(\omega) (\bar{n} + 1/2)}{|1 - \sqrt{\kappa} \chi_{aa}(\omega)|^{2} (\bar{n}_{L} + 1/2) + \kappa |\chi_{ab}(\omega)|^{2} (\bar{n} + 1/2)}.$$
(4.103)

The temporal modeshape that is optimally entangled to the mechanical oscillator is then given in the frequency domain by

$$u(\omega) = Nh(\omega), \tag{4.104}$$

where the normalisation constant N is

$$N = \left[\int_{-\infty}^{\infty} |h(t)|^2 dt \right]^{-1/2} = \sqrt{2\pi} \left[\int_{-\infty}^{\infty} |h(\omega)|^2 d\omega \right]^{-1/2}.$$
 (4.105)

The modeshape defined in Eq. (4.104) is shown in Fig. 4.14 for the specific case of $\bar{n}_L = \bar{n} = 0$ and an optomechanical cooperativity of C = 0.9. The main figure plots the modeshape in the frequency domain as a function of the ratio κ/Γ . It can be seen that, when $\Gamma \ll \kappa$, the filter is essentially a causal low-pass filter with a cut-off frequency of approximately Γ – that is, as might be expected, the temporal width of the optimal mode-shape is determined by the mechanical decay time. As Γ approaches and eventually exceeds κ , the modeshape is modified subtly due to the approach of the strong coupling regime, evidenced by the slight resonance feature in the bottom trace of the figure, and becomes increasingly noncausal.

The figure inset shows the optimal modeshape in the temporal domain for $\kappa/\Gamma=100$. As can be seen, the modeshape can be approximately described as a causal single-sided exponential with a decay rate of Γ . However, for this ratio of optical to mechanical decay rates, there still exists some noncausal contribution in the form of a forwards-in-time exponential of reduced amplitude. The causal contribution is larger because at time t the mechanical oscillator is correlated via the past radiation pressure to the optical field that entered the cavity prior to t, but is clearly not correlated to the optical field that enters the cavity subsequently. As a result, the optical field at times earlier than t carries a greater amount of information about the mechanical

oscillator and is weighted more strongly by the filter. It is this effect that, for sufficiently high optomechanical cooperativities and optical decay rates, results in an approximately causal filter.

From Eq. (4.98) we see that, in the frequency domain, the quadratures of the temporal mode u(t) are simply $\hat{X}_u(\omega) = u(\omega)\hat{X}_{L,\text{out}}(\omega)$ and $\hat{Y}_u(\omega) = u(\omega)\hat{X}_{L,\text{out}}(\omega)$ $u(\omega)\hat{Y}_{L,\mathrm{out}}(\omega)$. The covariance matrix elements between these quadratures and the mechanical oscillator can then be calculated in a similar manner as the intracavity case of Section 4.4.7, allowing quantification of the level of entanglement present between the two systems. The resulting logarithmic negativity is shown for $\kappa/\Gamma = 1000$ and various bath occupancies in Fig. 4.15. In the top figure, the mechanical bath occupancy is held fixed at $\bar{n}=0$ while the optical bath occupancy is increased from zero to, ultimately, infinity (dashed trace), showing that, for $\bar{n}=0$, the entanglement between the external cavity field and the mechanical oscillator is reduced as \bar{n}_L increases but is always present. In the bottom trace the optical occupancy is held fixed at $\bar{n}_L =$ 0. Again, we see that the entanglement is degraded as the mechanical bath occupancy increases. However, here, a threshold optomechanical cooperativity is introduced below which no entanglement is present. Since the system is unstable for C > 1, this ultimately introduces a maximum mechanical bath occupancy beyond which entanglement is only possible if some additional technique is introduced to stabilise the system.

It may seem surprising that, if the mechanical bath is in its ground state, the output optical field is always entangled to the mechanical oscillator independent of the optical occupancy \bar{n}_L . However, this can be understood in the following way. Consider an attempt to estimate the mechanical position quadrature X_M from a measurement of the field exiting the optomechanical system. As we have already discussed, the optimal estimate is given by $\hat{X}_M^{\text{est}}(t) = h_{X_M|Y_{L,\text{out}}}(t) * \hat{Y}_{L,\text{out}}(t), \text{ with an uncertainty of } \langle (\hat{X}_M(t) - \hat{X}_M^{\text{est}}(t))^2 \rangle.$ When the mechanical bath is in its ground state, the uncertainty of this estimate is smaller than the mechanical zero-point uncertainty for any choice of \bar{n}_L .

Exercise 4.21 Exercise. Show this result numerically, or otherwise.

As such, an optical phase quadrature measurement conditionally prepares a mechanical state with squeezed position quadrature (see Section 5.3.2 for further discussion of mechanical squeezed state preparation via measurement). Similarly, a measurement of the output optical amplitude quadrature conditionally prepares a momentum quadrature squeezed mechanical state. 17 The observables $\hat{u} = \hat{X}_M(t) - \hat{X}_M^{\text{est}}(t)$ and $\hat{v} = \hat{Y}_M(t) - \hat{Y}_M^{\text{est}}(t)$ then clearly exhibit joint uncertainty beneath the minimum uncertainty that is possible when only classical correlations are present (see Eq. (4.87) in Section 4.4.6), which, as we discussed in Section 4.4.6, is a sufficient criterion for entanglement.

¹⁷Note that, since \hat{X}_L and \hat{Y}_L cannot be measured simultaneously without a noise penalty, this does not allow the Heisenberg uncertainty principle to be violated.

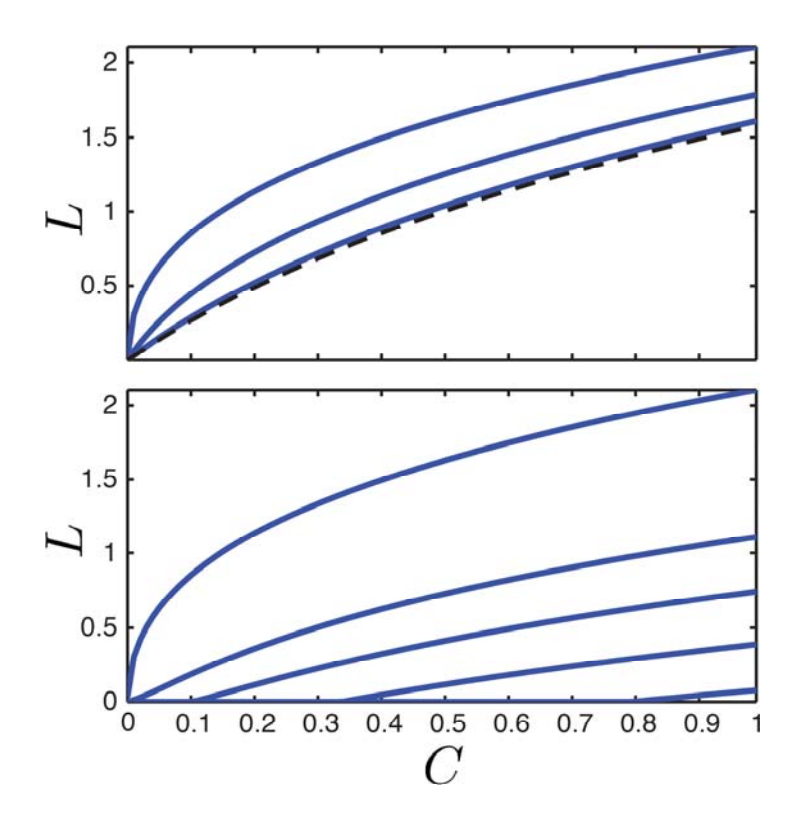


FIGURE 4.15 Logarithmic negativity of entanglement between mechanical oscillator and output optical field as a function of optomechanical cooperativity C, with $\kappa = 1000 \,\Gamma$. Top: Mechanical bath occupancy held fixed at $\bar{n} = 0$, with optical bath occupancy increasing over the range $\bar{n}_L = \{0, 1, 10\}$ from the top to bottom trace. Dashed line: logarithmic negativity as $\bar{n}_L \to \infty$. Bottom: Optical bath occupancy held fixed at $\bar{n}_L = 0$, with mechanical bath occupancy increasing over the range $\bar{n} = \{0, 1, 2, 4, 8\}$ from the top to bottom trace.

As mentioned above, optomechanical entanglement was first demonstrated in 2013 [217] using a lumped element superconducting microwave optomechanical system. In this implementation a pulsed optomechanics protocol was used [292], with an initial blue-detuned pulse generating entanglement and a second red-detuned pulse transferring the mechanical state out onto the microwave field. Ultimately, time-delayed entangled was observed between two microwave pulses. The experimental protocol and final covariance matrix are shown in Fig. 4.16.

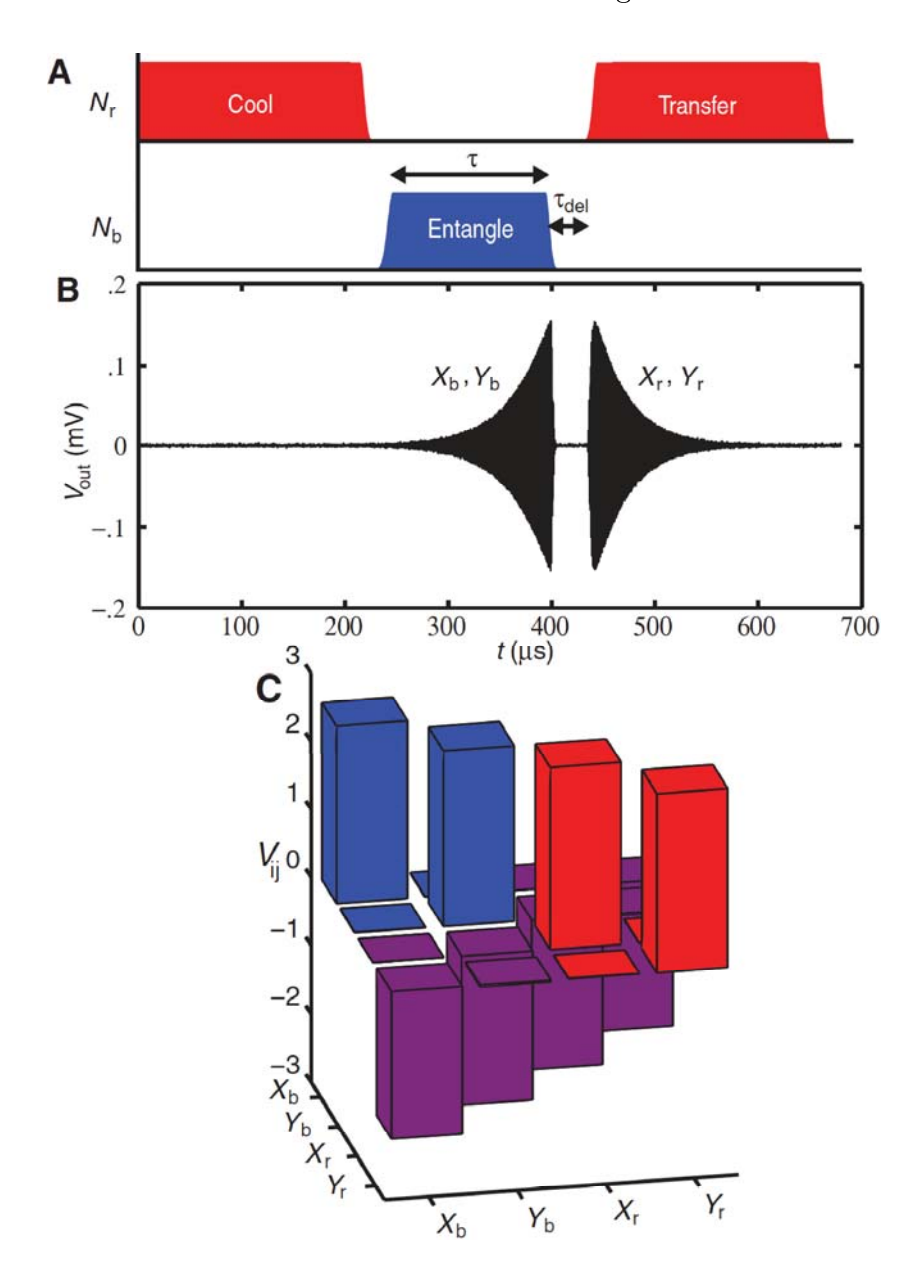
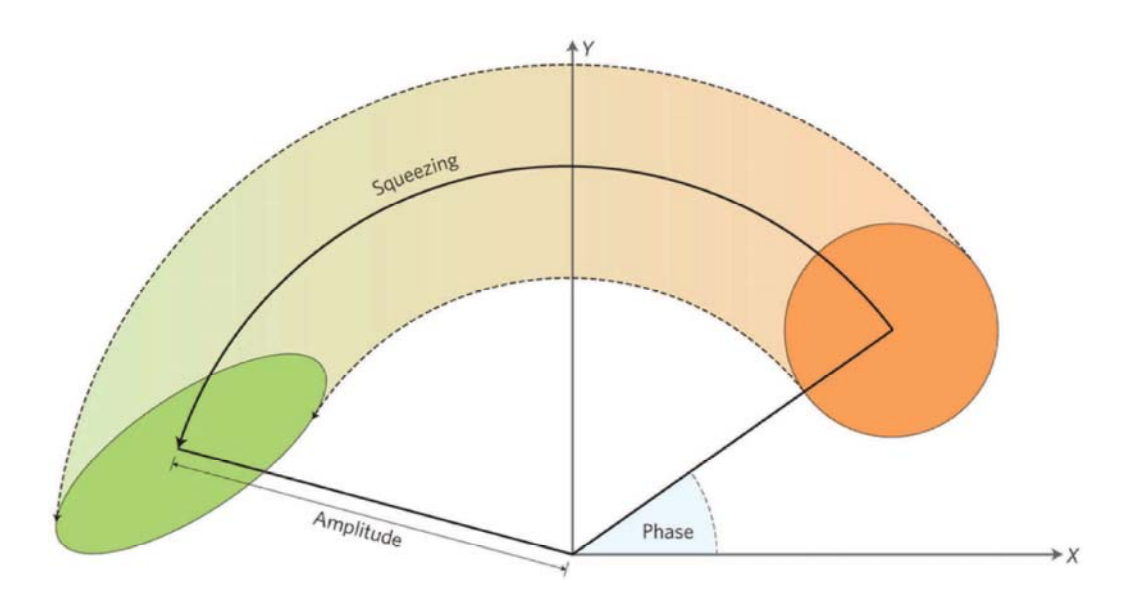


FIGURE 4.16 Optomechanical entanglement observed using a superconducting optomechanical system of the form shown in Fig. 2.2 (top left). From [217]. Reprinted with permission from AAAS. (A) Pulsed protocol to cool the mechanical oscillator, entangle it with a microwave field, and transfer the mechanical state out onto a second microwave field. (B) Detected microwave field as a function of time, showing the exponentially amplified initial entangled field leaving the microwave circuit followed by a second field as the mechanical motion is later transferred onto the intracavity field and decays out of the circuit. (C) Measured covariance matrix with off-diagonal elements evidencing entanglement. Here X_b and Y_b are the mechanical, and X_r and Y_r are the optical (or strictly speaking, microwave) quadrature operators.



Reprinted by permission from Macmillan Publishers Ltd: *Nature Photonics* [49], copyright 2013. The Kerr effect generates an intensity-dependent phase shift which skews the quantum noise distribution of light and can result in squeezing of the noise on one quadrature beneath the vacuum noise level.

4.5 MECHANICAL SQUEEZING OF LIGHT

From the perspective of the optical field, the optomechanical interaction imparts an intensity-dependent phase shift. The intensity of the optical field imparts momentum on the mechanical oscillator. This shifts its position, altering the phase of the optical field. Intensity-dependent phase shifts, or Kerr nonlinearities, are a common method to produce optical squeezing [263] (see Fig. 4.17) and can even generate optical states with Wigner negativity [329]. 18 It is therefore unsurprising that the optomechanical interaction is capable of producing squeezed light. However, there are some characteristic differences between this ponderomotive squeezing produced by interaction with a mechanical oscillator and squeezing produced by other nonlinear interactions that generate an intensity-dependent phase shift, such as the Kerr effect in optical fibres [260]. Most importantly, the mechanical resonance introduces strong dispersion to the squeezing spectra and restricts the bandwidth of squeezing, while coupling to the mechanical bath can introduce significant degradation on the levels of achievable squeezing. This section will quantitatively introduce mechanical squeezing of light and examine these effects in some detail.

¹⁸Though exceptionally strong nonlinearities are required to achieve this.

4.5.1 Basic concept

While ponderomotive squeezing is generally thought of as a continuous steadystate process, the basic idea may be understood by considering a pair of unitary interactions between the optical field and the mechanical oscillator. The essential goal is to introduce correlations between the optical amplitude and phase quadratures mediated by the mechanical oscillator. In the first unitary interaction the optical phase quadrature is displaced by a factor proportional to the mechanical position and the mechanical momentum is displaced by a factor proportional to the optical amplitude, i.e.,

$$\hat{Y}' = \hat{Y} + \lambda \hat{Q} \qquad (4.106a)$$

$$\hat{P}' = \hat{P} + \lambda \hat{X}, \qquad (4.106b)$$

$$\hat{P}' = \hat{P} + \lambda \hat{X}, \tag{4.106b}$$

where here λ is a proportionality constant that quantifies the strength of the interaction, and – since we treat ponderomotive squeezing without moving into a rotating frame for the mechanical oscillator – we have returned to our usual notation, with \hat{X} and \hat{Y} representing the optical amplitude and phase quadratures, and \hat{Q} and \hat{P} representing the mechanical position and momentum. The optical amplitude quadrature and mechanical position are left unaffected by the interaction.

If the mechanical oscillator is then allowed to evolve for a quarter of a cycle, the perturbed momentum rotates into a position, $\hat{Q}'' = -\hat{P}'$. A second interaction of the same form as Eq. (4.106) then results in the final optical quadratures

$$\hat{X}'' = \hat{X} \tag{4.107a}$$

$$\hat{X}'' = \hat{X}$$

$$\hat{Y}'' = \hat{Y} + \lambda \left(\hat{Q} - \hat{P}\right) - \lambda^2 \hat{X}.$$
(4.107a)
$$(4.107b)$$

We see that this series of interactions imprints the optical amplitude quadrature onto the optical phase quadrature, introducing a correlation, and also imprints the original mechanical position and momentum operators on the light. It is introducing exactly the intensity (or amplitude) dependent phase shift we expect of an optical Kerr nonlinearity. This shears the distribution of quantum noise on the optical field in a similar way to the illustration in Fig. 4.17.

Given the correlations between \hat{X}'' and \hat{Y}'' , there will exist some rotated quadrature of the optical field $\hat{Y}^{"\theta}$ where \hat{X} is eliminated.

Exercise 4.22 Using the definition of the rotated operator in Eq. (1.17b), which applies equally well to the phase quadrature operator as to the dimensionless momentum operator, show that \hat{X} is eliminated on the \hat{Y}'' quadrature when $\tan \theta = -\lambda^2$, and that choosing this quadrature angle,

$$\hat{Y}^{"\theta} = \frac{\hat{Y} + \lambda \left(\hat{Q} - \hat{P}\right)}{\sqrt{\lambda^4 + 1}}.$$
(4.108)

It is evident from this expression that, even including the mechanical position and momentum fluctuations, as the interaction strength $\lambda \to \infty$, the variance of $\hat{Y}^{"\theta}$ will approach zero, in principle allowing perfect optical squeezing.

4.5.2 Understanding ponderomotive squeezing via the polaron transformation

The intuition that a continuous optomechanical interaction can be thought of, from the perspective of the light, as a Kerr nonlinearity can be put on a solid foundation by making use of the polaron transformation to diagonalise the optomechanical Hamiltonian \hat{H} . This approach is common in condensed matter physics where it is useful to treat problems involving linear coupling between electrons and phonons (see, for example, [187]). The essential idea is to apply a displacement to the mechanical oscillator that corrects for the shift in the mechanical oscillator equilibrium position due to the interaction with the optical field.

The magnitude of the displacement due to the optomechanical interaction may be found, for example, by completing the square on the full (nonlinearised) Hamiltonian of Eq. (2.18).

Exercise 4.23 Show that, to third order in the operators, ¹⁹ Eq. (2.18) may be re-expressed as

$$\hat{H} = \hbar \Delta a^{\dagger} a + \frac{\hbar \Omega}{2} \left[\hat{P}^2 + \left(\hat{Q} + \frac{\sqrt{2}g_0}{\Omega} a^{\dagger} a \right)^2 \right]. \tag{4.109}$$

This expression makes clear that the radiation pressure interaction displaces the dimensionless mechanical position by $-\sqrt{2}g_0a^{\dagger}a/\Omega$, consistent with our mean field observations from Chapter 2.

4.5.2.1 Polaron transformation

In the polaron transformation, one cancels this displacement by applying an opposite but equivalent displacement via the unitary operator

$$\hat{S} = \exp\left[i\frac{\sqrt{2}g_0}{\Omega}a^{\dagger}a\hat{P}\right]. \tag{4.110}$$

The Hamiltonian of Eq. (2.18) is then transformed to

$$\hat{\bar{H}} \equiv \hat{S}^{\dagger} \hat{H} \hat{S} \tag{4.111}$$

$$= \hbar \Delta a^{\dagger} a - \hbar \chi_0 \left(a^{\dagger} a \right)^2 + \frac{\hbar \Omega}{2} \left(\hat{Q}^2 + \hat{P}^2 \right), \tag{4.112}$$

 $^{^{19}\}mathrm{By}$ this we mean neglecting any terms that involve the product of more than three operators.

where we have defined the single-photon optical frequency shift

$$\chi_0 \equiv \frac{g_0^2}{\Omega},\tag{4.113}$$

and identify operators in the polaron frame via the bar accent. As we will see in Chapter 6, this is an important parameter for single-photon optomechanics.

Exercise 4.24 Show that

$$\hat{\bar{Q}} \equiv \hat{S}^{\dagger} \hat{Q} \hat{S} = \hat{Q} - \frac{\sqrt{2}g_0}{\Omega} a^{\dagger} a, \tag{4.114}$$

making use of the Hadamard lemma

$$e^{\hat{A}}\hat{B}e^{-\hat{A}} = \hat{B} + [\hat{A}, \hat{B}] + \frac{1}{2!}[\hat{A}, [\hat{A}, \hat{B}]] + \frac{1}{3!}[\hat{A}, [\hat{A}, [\hat{A}, \hat{B}]]] + \dots$$

Then derive the polaron transformed Hamiltonian of Eq. (4.112) from Eq. (2.18), using the general property of a unitary operator \hat{U} that $\hat{U}^{\dagger}\hat{A}\hat{B}\hat{U} = \hat{U}^{\dagger}\hat{A}\hat{1}\hat{B}\hat{U} = \hat{U}^{\dagger}\hat{A}\hat{U}\hat{U}^{\dagger}\hat{B}\hat{U}$, where 1 is the identity operator.

This new Hamiltonian makes a number of things transparent about the optomechanical interaction. Most particularly, we see that the dynamics of the mechanical oscillator and intracavity field are now independent. The optomechanical interaction term in Eq. (2.18) has been replaced with the photon-photon interaction term $\chi_0 \left(a^{\dagger}a\right)^2$ characteristic of a pure optical Kerr nonlinearity with no dependence on the dynamics of the mechanical oscillator. Notice that this term is proportional to g_0 squared, since the effective photon-photon interaction involves two interactions with the mechanical oscillator, one to drive the motion of the oscillator and the other to transduce the motion back onto the optical field.²⁰ This conversion of an optomechanical nonlinearity to a purely optical one was the primary purpose of the polaron transformation. In the absence of other nonlinear terms in the Hamiltonian, it is well known that the optical Kerr nonlinearity is capable of generating squeezed states of light [328, 263, 260] and even, in principle, Schrödinger's cat-like states [329].

4.5.2.2 Squeezing action in the polaron picture

We can understand why a term proportional to $(a^{\dagger}a)^2$ will generate squeezing of the optical field by expanding and linearising this term, replacing $a \to \alpha + a$ and neglecting terms that are lower than second order in α :

$$(a^{\dagger}a)^2 \to \alpha^4 + \alpha^2 + 2\alpha^3(a^{\dagger} + a) + 4\alpha^2 a^{\dagger}a + \alpha^2(a^{\dagger 2} + a^2).$$
 (4.115)

The first two terms in this expansion are static and have no effect on the dynamics of a, the third is a displacement, and the fourth a frequency shift.

²⁰As we saw in our toy example in Section 4.5.1.

144 ■ Quantum optomechanics

The last term can be seen to produce correlated pairs of photons within the cavity. It is this term that is responsible for squeezing the intracavity field. Using Eqs. $(1.17)^{21}$ we can reexpress

$$a^{\dagger 2} + a^2 = -4\hat{X}^{\pi/4}\hat{Y}^{\pi/4} \tag{4.116}$$

within a constant, where $\hat{X}^{\pi/4}$ and $\hat{Y}^{\pi/4}$ are quadrature operators that are rotated by $\pi/4$ from the amplitude and phase quadratures. Setting the overall cavity detuning to zero, including the shift from Eq. (4.115), and neglecting the static and displacement terms from Eq. (4.115), the linearised Hamiltonian describing the intracavity field is then simply

$$\hat{\bar{H}} = 4\hbar\chi \hat{X}^{\pi/4} \hat{Y}^{\pi/4}, \tag{4.117}$$

where $\chi \equiv \chi_0 \alpha$ is the coherent amplitude boosted optical frequency shift. This is the classical Hamiltonian for parametric squeezing.

Exercise 4.25 Using the quantum Langevin equation of Eq. (1.112) show that this Hamiltonian acts to amplify the $\hat{X}^{\pi/4}$ quadrature while deamplifying (and therefore squeezing) the $\hat{Y}^{\pi/4}$ quadrature.

4.5.2.3 Interaction with the coherent drive and the optical and mechanical baths

While the above discussion appears to suggest that, by performing a polaron transformation, we have found an exceptionally simple method to model ponderomotive squeezing, unfortunately this is not the case. While the polaron transform diagonalises the system Hamiltonian, it introduces coupling between the mechanical oscillator and the optical field through its effect on the drive and system-bath interaction Hamiltonians. This can be seen straightforwardly by applying the polaron transformation to the drive term in the Hamiltonian of Eq. (2.35).

Exercise 4.26 Using the same approach as in Exercise 4.24 show that

$$\bar{a} \equiv \hat{S}^{\dagger} a \hat{S} = a \exp\left[i \frac{\sqrt{2}g_0}{\Omega} \hat{P}\right],$$
 (4.118)

and therefore that, in the polaron frame, the drive term in Eq. (2.35) is dependent on the mechanical momentum quadrature \hat{P} .

Similarly, applying the polaron transformation to the system-bath terms in Eqs. (1.69) and (1.111) one finds that, in the polaron frame, the system-bath coupling terms introduce a new optomechanical interaction, with the coupling

²¹These equations can be applied to the quadrature operators as well as the dimensionless position and momentum, with $\hat{Q} \to \hat{X}$ and $\hat{P} \to \hat{Y}$.

rate between the optical field and its bath dependent on the mechanical position. This is a form of dissipative optomechanical coupling, as discussed in Section 2.8. A linear coupling is also introduced between the intracavity optical field and the mechanical bath. This coupling is direct – i.e., it is not mediated by the mechanical oscillator.

Overall, these effects mean that, while the polaron transformation is useful for understanding the unitary dynamics of ponderomotive squeezing, it does not yield significant benefits for modelling the nonunitary dynamics. We return to the polaron transformation in Chapter 6, where it proves to be highly useful for studying quantum optomechanics at the single-photon level. Henceforth in this section, we use the usual optomechanical Hamiltonian.

4.5.3 Squeezing spectra

In Sections 3.2 and 3.3 we examined radiation pressure shot noise heating of a mechanical oscillator and the standard quantum limit to measurements of mechanical motion using the linearised optomechanical Hamiltonian of Eq. (2.41) in the zero detuning limit. However, in those sections we examined only the effect of the quantum noise of the light on the temperature of the mechanical oscillator and the information contained on the phase quadrature of the output optical field about the mechanical motion. We did not look at correlations induced by radiation pressure between the amplitude and phase of the output optical field.

While it is possible to generate ponderomotive squeezing in the general case where $\Delta \neq 0$, here, for simplicity, we again restrict ourselves to the zero detuning case. 22 To examine correlations in the output field, we must express the output optical phase quadrature \hat{Y}_{out} in terms of the optical and mechanical input fluctuations. This is straightforward to do using Eqs. (3.29b) and (3.12), with the result

$$\hat{Y}_{\text{out}}(\omega) = -\left(\frac{\kappa/2 + i\omega}{\kappa/2 - i\omega}\right) \hat{Y}_{\text{in}}(\omega) + 2\Gamma\chi(\omega) \left[\sqrt{2C_{\text{eff}}}\hat{P}_{\text{in}}(\omega) - 2C_{\text{eff}}\hat{X}_{\text{in}}(\omega)\right],$$
(4.119)

where we have returned to our usual definitions of the optical amplitude and phase quadratures (\hat{X} and \hat{Y} , respectively) and dimensionless position and momentum operators (\hat{Q} and \hat{P} , respectively). We see that, through the optomechanical interaction, the input fluctuations of the optical amplitude quadrature are imprinted on the output optical phase quadrature, just as we found earlier for the simple model of two discrete and temporally separated interactions (Section 4.5.1). This induces correlations that are at the heart of ponderomotive squeezing. It should be noted that the correlations are enhanced close to the mechanical resonance due to the mechanical susceptibility pre-factor $\chi(\omega)$. Furthermore, as the optomechanical cooperativity C_{eff} in-

²²The case of nonzero detuning displays the same qualitative behaviour.

creases, the contribution from the optical amplitude increases at a faster rate than that from mechanical input fluctuations.

Using Eq. (4.119) in combination with the output optical amplitude given in Eq. (3.29a), an arbitrary output quadrature at phase angle θ may be determined via Eq. (1.17a), with the result

$$\hat{X}_{\text{out}}^{\theta}(\omega) = -\left[\left(\frac{\kappa/2 + i\omega}{\kappa/2 - i\omega}\right) \cos\theta + 4\Gamma C_{\text{eff}}\chi(\omega) \sin\theta\right] \hat{X}_{\text{in}}(\omega) \qquad (4.120)$$
$$-\left(\frac{\kappa/2 + i\omega}{\kappa/2 - i\omega}\right) \sin\theta \, \hat{Y}_{\text{in}}(\omega) + 2\Gamma \sqrt{2C_{\text{eff}}}\chi(\omega) \sin\theta \, \hat{P}_{\text{in}}(\omega).$$

The symmetrised power spectral density that would be measured via perfect homodyne detection can then be calculated using Eqs. (1.65) and (1.99) and is given by

$$\bar{S}_{X_{\text{out}}^{\theta}X_{\text{out}}^{\theta}}(\omega) = \frac{1}{2} + 8\Gamma^{2}|\chi(\omega)|^{2}|C_{\text{eff}}|\left(\bar{n} + |C_{\text{eff}}| + \frac{1}{2}\right)\sin^{2}\theta + \Gamma|C_{\text{eff}}|\left(\chi(\omega) + \chi^{*}(\omega)\right)\sin 2\theta, \tag{4.121}$$

where for simplicity we have taken the output field to be shot noise limited $(\bar{n}_L = 0)$. The first term is the original quantum noise on the quadrature in the absence of any optomechanical interaction. The second term is a form of mechanical heating proportional to the variance of the mechanical position in the presence of radiation pressure driving and is always positive. The third and final term is the correlation term responsible for ponderomotive squeezing and gives the power spectral density a Fano-like shape. For the output quadrature to exhibit quantum squeezing below the shot noise level (1/2), this term must be negative and have a magnitude larger than the second term. This leads to the necessary and sufficient condition for quantum squeezing $(\bar{S}_{X_{\text{out}}^{\theta}X_{\text{out}}^{\theta}}(\omega) < 1/2)$,

$$\bar{n} + |C_{\text{eff}}| + \frac{1}{2} < \frac{\Omega^2 - \omega^2}{2\Gamma\Omega \tan \theta},\tag{4.122}$$

where we have made use of the definition of the mechanical susceptibility given in Eq. (1.102). Thus we see that quantum squeezing cannot occur exactly on the mechanical resonance ($\omega = \Omega$). By contrast, at all other frequencies quantum squeezing is always present for some range of phase angles θ , since for any frequency $\omega \neq \Omega$ the right-hand side of Eq. (4.122) goes to infinity as $\theta \to 0$ from either above or below. We can further observe that, for a given phase angle θ , squeezing will only exist on one side of the mechanical resonance frequency, with the side showing squeezing dictated by the sign of $\tan \theta$. The ponderomotive squeezing predicted from Eq. (4.121) is plotted for a range of parameters in Fig. 4.18a and b, showing this asymmetric frequency response around the mechanical resonance.

Minimising Eq. (4.121) over θ yields the optimal angle θ_{opt} to achieve

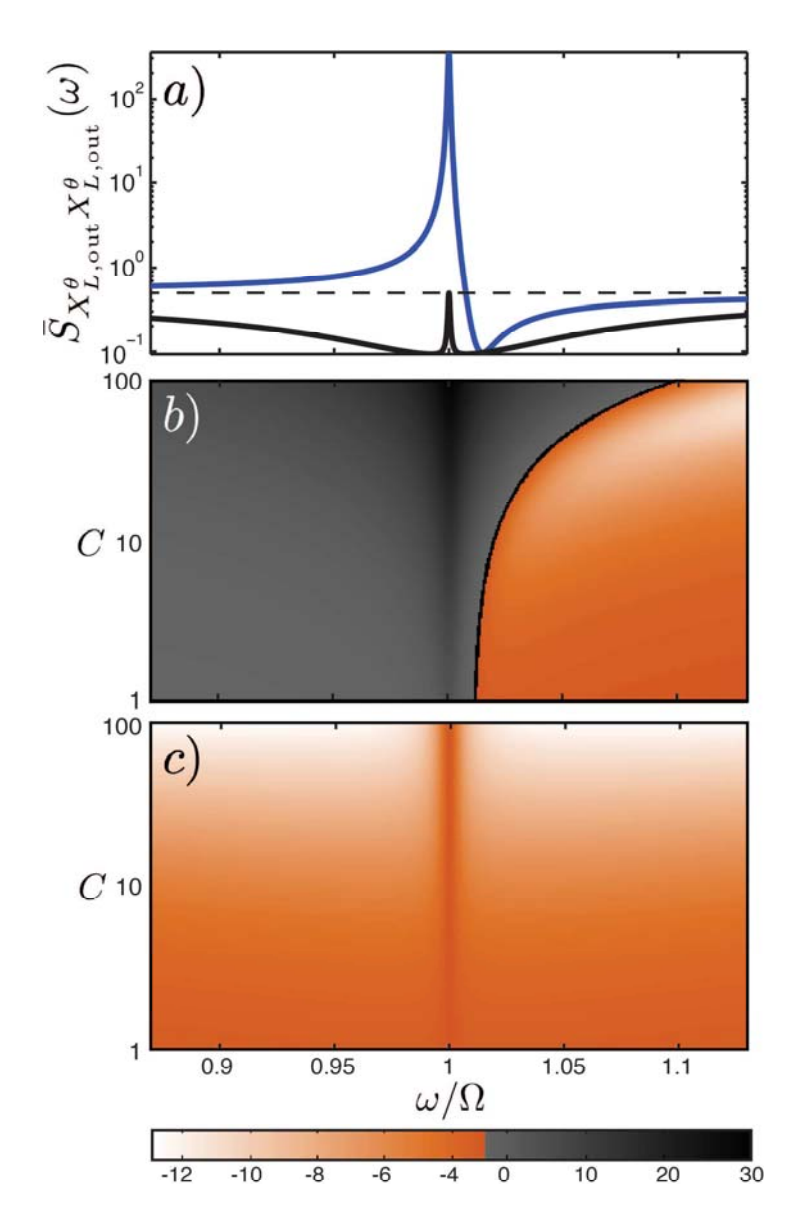


FIGURE 4.18 Theoretical model of ponderomotive squeezing, using the parameters $\kappa/\Omega=10,\,\bar{n}=10,\,{\rm and}\,\,Q=1,000.$ (a) Squeezing as a function of frequency ω for an optomechanical cooperativity of C=50. Top trace: power spectral density of the output quadrature $\bar{S}_{X_{L,\text{out}}^{\theta}X_{L,\text{out}}^{\theta}}(\omega)$ with phase angle $\theta = \pi/25$. Bottom trace: power spectral density choosing the optimal phase angle $\theta_{\rm opt}(\omega)$ for each frequency. Dashed line: shot noise level. (b) $10 \log_{10} \{ \bar{S}_{X_{L,\text{out}}^{\theta} X_{L,\text{out}}^{\theta}}(\omega) \}$ as a function of frequency and optomechanical cooperativity for $\theta = \pi/25$. Solid trace: contour of $\bar{S}_{X_{L,\text{out}}^{\theta}X_{L,\text{out}}^{\theta}}(\omega)=1/2$. (c) $10\log_{10}\{\bar{S}_{X_{L,\text{out}}^{\theta}X_{L,\text{out}}^{\theta}}(\omega)\}$ as a function of frequency and optomechanical cooperativity choosing the optimal phase angle $\theta_{\rm opt}(\omega)$.

maximum squeezing, given by

$$\tan 2\theta_{\text{opt}} = \frac{\omega^2 - \Omega^2}{2\Gamma\Omega \left(n + |C_{\text{eff}}| + 1/2\right)}.$$
(4.123)

We see that the squeezing angle rotates as a function of frequency, crossing zero at the mechanical resonance frequency. The optimal squeezing at each frequency is shown for a range of parameters in Fig. 4.18a and c. We observe that, indeed, no squeezing is possible on the mechanical resonance, while broadband squeezing is achieved, in principle, over all other frequencies, with the level of squeezing increasing with effective cooperativity. The ponderomotive squeezing is resonantly enhanced near the mechanical resonance frequency, such that substantial levels of squeezing typically only exist in a relatively narrow band of frequencies. This contrasts techniques to generate squeezed light using standard nonlinear optical materials which are able to routinely generate broadband squeezing.

As we will see in Section 5.4.3, the ability to generate squeezing via the optomechanical interaction provides one path to overcome the standard quantum limit introduced in Section 3.4. However, as will be discussed in that section, the squeezing angle rotation evident in Eq. (4.123) complicates this approach to sub-standard quantum limited measurement, resulting in noise suppression only in a small band of frequencies unless specialised measurement techniques referred to as *variation measurements* are employed (see Fig. 5.9).

Ponderomotive squeezing was first proposed in 1994 [103, 189] and first demonstrated in 2012 [52]. It has been observed in several optomechanical architectures including intracavity cold atom ensembles [52], silicon nitride membrane optomechanical systems [232], and optomechanical zipper cavities [245]. Figure 4.19 shows an optomechanical zipper cavity and the observed optical power spectrum for a fixed homodyne phase angle. It can be observed that the power spectrum exhibits the expected Fano-like feature, with a small region of quantum squeezing observed at frequencies just below the mechanical resonance frequency.

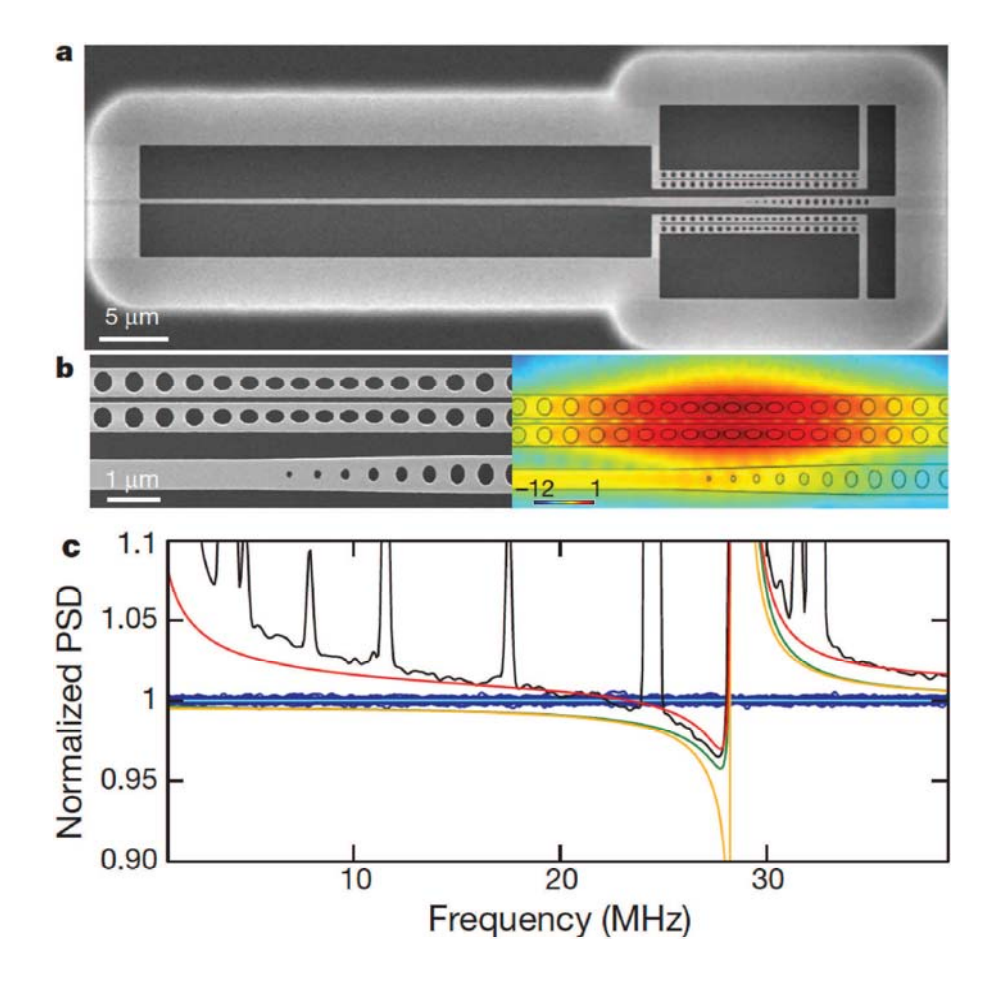


FIGURE 4.19 Ponderomotive squeezing observed from an optomechanical zipper cavity. Adapted by permission from Macmillan Publishers Ltd: Nature [245], copyright 2013. (a) and (b) Scanning electron micrscope images and optical modelling of the zipper cavity structure. (c) Optical power spectral density observed for one homodyne phase angle and normalised to the shot noise level. PSD: power spectral density of output field.